PCCP

PAPER

Cite this: *Phys. Chem. Chem. Phys.*, 2018, **20**, 562

Correlating geminal $^2J_{Si-O-Si}$ couplings to structure in framework silicates†

D. J. Srivastava,[a] P. Florian,[b] J. H. Baltisberger[c] and P. J. Grandinetti *[a]

Received 21st September 2017,
Accepted 21st November 2017

DOI: 10.1039/c7cp06486a

rsc.li/pccp

The dependence of a ^{29}Si geminal *J* coupling across the inter-tetrahedral linkage on local structure was examined using first-principles DFT calculations. The two main influences on $^2J_{Si-O-Si}$ were found to be a primary dependence on the linkage Si–O–Si angle and a secondary dependence on mean Si–O–Si linkage of the two coupled ^{29}Si nuclei. An analytical expression describing these dependences was proposed and used to develop an approach for relating the correlated pair of $^2J_{Si-O-Si}$ coupling and mean ^{29}Si isotropic chemical shift to the linkage Si–O–Si angle and the mean Si–O–Si angle of the two coupled ^{29}Si nuclei. An example of this analysis is given using ^{29}Si NMR results from the siliceous zeolite Sigma-2.

1 Introduction

The isotropic chemical shift of ^{29}Si NMR has long been a valuable probe of structure in silicate materials.[1–4] In changing coordination from SiO_4 to SiO_5 to SiO_6 the chemical shift range of ^{29}Si in silicates varies from approximately −100 to −150 to −200 ppm, respectively.[5] In the case of tetrahedral coordination, the chemical shift varies over a range of −120 to −70 ppm as the second coordinate sphere changes from fully connected Q^4 to fully disconnected Q^0, respectively.[6] For Q^4 sites it is well established that variations in the range of −105 ppm to −120 ppm in the isotropic chemical shift of ^{29}Si are correlated to the mean of the Q^4's four inter-tetrahedral angles.[7–9]

The anisotropy of the ^{29}Si chemical shift is also strongly correlated to changes in the first-coordination sphere. As first noted by Grimmer and coworkers,[10,11] as the Si–O bond length decreases there is an increase in the s-character of the bonding orbital at Si and corresponding increase in shielding along the direction of the shorter bond. This strong dependence of the ^{29}Si chemical shift anisotropy has been exploited not only for distinguishing and quantifying Q^n sites,[12–16] but recently has been found to be an effective probe of the modifier cation coordination to the non-bridging oxygen of Q^3 sites[17] and useful in the NMR refinement of crystal structures.[18]

In contrast to the ^{29}Si chemical shift, accurate measurements of geminal $^2J_{Si-O-Si}$ couplings across the inter-tetrahedral linkage in silicates have yielded no clear relationships between coupling constant and local structure. While $^2J_{Si-O-Si}$ couplings in solution have been measured,[19–23] motional averaging makes it difficult to use these measurements to establish empirical relationships. The number of $^2J_{Si-O-Si}$ measurements in solids have been limited, particularly at ^{29}Si natural abundance levels, 4.67%, and thus far few efforts[24–26] have been made in trying to establish quantitative relationships between $^2J_{Si-O-Si}$ and structure. Compounding this issue is that commercial computational chemistry packages have only recently reached the level where accurate *J*-couplings can be calculated through using expensive density function theory (DFT) methods.[27] Nevertheless, geometric dependences have been reproduced using modest DFT calculations. The most recent attempts in determining such relationships, using *ab initio* DFT methods, were in 2009 by Cadars *et al.*[26] and Florian *et al.*[25] Although both groups acknowledged a dependence of $^2J_{Si-O-Si}$ coupling on Si–O–Si bond angle, Florian *et al.* suggested a one-to-one mapping, whereas Cadars *et al.* found that the dependence of the $^2J_{Si-O-Si}$ coupling is not limited to the Si–O–Si bond angle but is also influenced significantly by the local geometry around the Si–O–Si linkage. Cadars *et al.* concluded that such dependencies led to a relatively "large scatter" of $^2J_{Si-O-Si}$ coupling, with respect to Si–O–Si bond angle, and did not attempt to deduce any empirical relationship between the $^2J_{Si-O-Si}$ coupling and the local structure. To get a sense of that scatter, we plot the $^2J_{Si-O-Si}$ couplings—calculated here—as a function of Si–O–Si bond angle in Fig. S5 of the ESI.†

Here we re-examine the variation in $^2J_{Si-O-Si}$ using Q^4–Q^4 clusters that are centered on the Si–O–Si linkage extending out to four coordination spheres away from the bridging oxygen between the two coupled silicon. With greater computational resources than were available to Cadars *et al.* 8 years ago,

[a] *Department of Chemistry and Biochemistry, 100 West 18th Avenue, Columbus, OH, USA. E-mail: grandinetti.1@osu.edu*
[b] *CNRS, UPR3079 CEMHTI, 1D Avenue de la Recherche Scientifique, 45071 Orléans Cedex 2, France*
[c] *Division of Natural Science, Mathematics, and Nursing, Berea College, Berea, KY, USA*

† Electronic supplementary information (ESI) available. See DOI: 10.1039/c7cp06486a

we were able to increase the level of theory and obtain excellent agreement with known experimental $^2J_{Si-O-Si}$ couplings. Through systematic structural variations of the cluster, we investigated the influence of (1) the Si–O–Si linkage angle, (2) the Si–O bond distance, (3) the inter-tetrahedral dihedral angle, and (4) the outer Si–O–Si linkage angles of the two coupled ^{29}Si nuclei. Most significantly we show here that after the central Si–O–Si linkage angle it is the outer Si–O–Si linkage angles of the Q^4–Q^4 couple that play the next most significant role in determining $^2J_{Si-O-Si}$. A smaller dependence on the dihedral angle is observed while a negligible dependence on Si–O distance over relevant length scales is observed. In this study we assume the SiO_4 tetrahedron does not deviate from local tetrahedral symmetry and take the intra-tetrahedral O–Si–O angle as constant. While this is a reasonable approximation in a fully connected Q^4 network, it is likely that this assumption will break down as the silicate network becomes depolymerized. Further work will be required to understand the dependence of J coupling on local structure in networks having significant distortions around SiO_4 tetrahedra.

As the isotropic chemical shift has a well known dependence on the mean Si–O–Si angle, we also show here that a correlation plot of mean ^{29}Si isotropic chemical shift *versus* $^2J_{Si-O-Si}$ coupling can be mapped into a two dimensional structural correlation of linkage Si–O–Si angle to mean Si–O–Si angle of the two coupled ^{29}Si nuclei.

2 Method

All *ab initio* calculations were carried out using Gaussian 09[28] at the Ohio supercomputing center,[29] running HP SL390 G7 two-socket servers with Intel Xeon x5650 (Westmere-EP, 6 core, 2.67 GHz) processors and 48 GB memory. The natural atomic orbital and natural bond orbital analysis was performed using Gaussian NBO version 3.1.[30] The $^2J_{Si-O-Si}$ couplings were calculated using DFT with B3LYP functional on a small O centered SiH_3 terminated cluster, $(H_3SiO)_3$–Si–O–Si–$(OSiH_3)_3$, shown in Fig. 1. A perfect tetrahedron angle $\angle$ O–Si–O = 109.5° was imposed about Si atoms in all calculations.

A locally dense basis set was implemented on this cluster, as suggested by Cadars *et al.*,[26] for accurate $^2J_{Si-O-Si}$ coupling calculations. This follows an implementation of cc-PV5Z basis set on the two central Si (labeled $Si^{(i)}$ and $Si^{(j)}$ in Fig. 1), 6-31++G basis set on all H, and 6-31++G* basis set on all O and remaining Si. Single point NMR calculations were run with tight self consistent field (SCF) convergence criteria. The integration grid size was increased to a pruned (99, 590), '*ultrafine*' grid, although no differences in $^2J_{Si-O-Si}$ couplings were observed from the pruned (75, 302) '*fine*' integration grid. All further calculations were, therefore, subjected to a '*fine*' integration grid. With this setup each calculation took approximately four and a half hours split over 12 cpu cores.

Systematic structural variations of the cluster were performed to investigate the $^2J_{Si-O-Si}$ coupling dependence on and correlations between the central Si–O–Si bond angle, Ω_0, and (a) Si–O bond distances, d_{Si-O}, (b) O–Si–Si–O inter-tetrahedral dihedral bond angle, ϕ (index O_1–$Si^{(i)}$–$Si^{(j)}$–O_4 in Fig. 1) and (c) outer

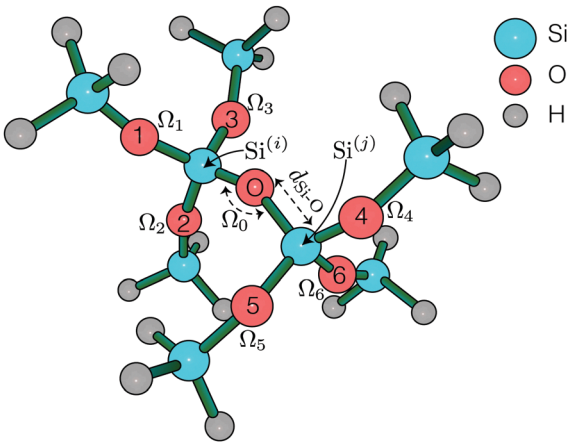

Fig. 1 $(H_3SiO)_3$–Si–O–Si–$(OSiH_3)_3$ symmetric cluster used in calculating the $^2J_{Si-O-Si}$ coupling across $Si^{(i)}$–O–$Si^{(j)}$.

Si–O–Si bond angles (Ω_1 to Ω_6). With the geometry constrained out to the third coordination sphere of the central linkage oxygen, a geometry optimization of the outermost Si–H bond distances and the remaining dihedral angles was performed once using restricted Hartree–Fock, RHF/6-311G(d) basis set. We found, as did Cadars *et al.*,[26] that variations in these fourth coordination sphere geometries had negligible effect on the predicted J-coupling. We confirmed this finding with several $^2J_{Si-O-Si}$ coupling calculation starting with RHF/6-311G(d) optimized initial geometries and the results are tabulated in Table S3 of the ESI.† A complete list of all geometrical constraints imposed in this study is tabulated in Tables S1–S5 of the ESI.†

Si–O bond distance, d_{Si-O}

The $^2J_{Si-O-Si}$ coupling dependence on and correlation between Ω_0 and d_{Si-O} was explored by performing a series of $^2J_{Si-O-Si}$ coupling calculations on the optimized structure by varying Ω_0 from 120° to 180° on a uniform grid for three Si–O bond distances, d_{Si-O} = 1.58 Å, 1.60 Å and 1.62 Å, respectively, Fig. 2C.

O–Si–Si–O dihedral angle, ϕ

A similar series of calculations were performed on the optimized geometry to investigate the $^2J_{Si-O-Si}$ coupling dependence on and correlation between Ω_0 and ϕ. This was accomplished by independently varying ϕ and Ω_0 from −60° to +60° and 120° to 180°, respectively, Fig. 2B. All Si–O bond distances were set to 1.6 Å.

Outer Si–O–Si bond angle, $\Omega_{k\neq 0}$

A complete systematic exploration of the $^2J_{Si-O-Si}$ dependence on the six outer Si–O–Si bond angles would have exceeded our computational capabilities. In light of the well established[8] linear dependence of the isotropic ^{29}Si chemical shift on the mean Si–O–Si bond angle for a Q^4 tetrahedra we attempted to reduce the dimensionality of the problem by using the mean Si–O–Si bond angle for each Q^4 tetrahedra, ($Si^{(i)}$ and $Si^{(j)}$) involved in the $^2J_{Si-O-Si}$ coupling, that is,

$$\langle\Omega\rangle_i = \frac{1}{4}\sum_{k=0,1,2,3}\Omega_k, \text{ and } \langle\Omega\rangle_j = \frac{1}{4}\sum_{k=0,4,5,6}\Omega_k, \qquad (1)$$

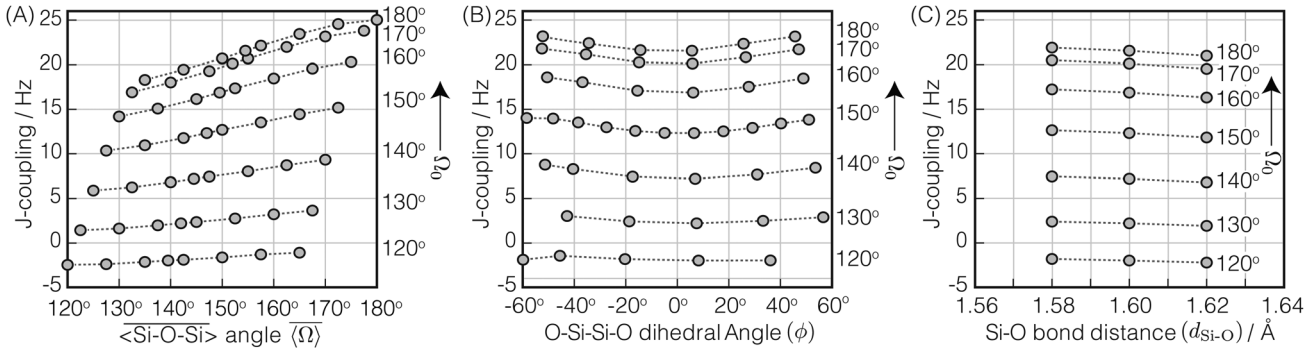

Fig. 2 Dependence and correlation of $^2J_{Si-O-Si}$ couplings between $Si^{(i)}$–O–$Si^{(j)}$ bond angle, Ω_0 and (A) $\overline{\langle\Omega\rangle}$, (B) O–Si–Si–O inter tetrahedral dihedral angle, ϕ and (C) Si–O bond distance, d_{Si-O}. For calculations in (A) d_{Si-O} = 1.60 Å and $\Omega_{k\neq0} = \Omega_{out}$ varied from 120° to 180°. In (B) d_{Si-O} = 1.60 Å, Ω_{out} = 146° and ϕ varied from −60° to +60°. In (C) Ω_{out} = 146° and d varied from 1.58 Å to 1.62 Å.

to calculate a double mean

$$\overline{\langle\Omega\rangle} = \frac{\langle\Omega\rangle_i + \langle\Omega\rangle_j}{2} = \frac{1}{8}\left(2\Omega_0 + \sum_{k=1}^{6}\Omega_k\right). \quad (2)$$

Through systematic variation of Ω_0 (the central linkage angle) and $\overline{\langle\Omega\rangle}$ we show (*vide infra*) that a combined measurement of isotropic ^{29}Si chemical shift and $^2J_{Si-O-Si}$ can be exploited to determine the local structure around the Q^4–Q^4 linkage.

Despite this effort to reduce the dimensionality of this problem from seven to two, there still exist infinite combinations of $\Omega_{k\neq0}$ that lead to the same $\overline{\langle\Omega\rangle}$ in eqn (2), with the exception of the singular—and highly unlikely—occurrence of $\overline{\langle\Omega\rangle} = 180^\circ$. To ensure a systematic variation of the local structure, we choose to constrain all $\Omega_{k\neq0} = \Omega_{out}$. A series of $^2J_{Si-O-Si}$ calculations were performed by independently vary Ω_{out} and Ω_0 from 120° to 180° on a uniform grid. The calculated $^2J_{Si-O-Si}$ as a function of $\overline{\langle\Omega\rangle}$ and Ω_0 is presented in Fig. 2A. All Si–O bond distances were set to 1.6 Å. Of course, the constraint $\Omega_{k\neq0} = \Omega_{out}$, implemented only to ensure a systematic local structural variation, is unrealistic even for most crystalline silicates and highly siliceous zeolites, as well as in silica glass and other silica rich disordered materials. To break free from this constraint numerous $^2J_{Si-O-Si}$ coupling calculations were performed at arbitrary outer Si–O–Si bond angles $\Omega_{k\neq0}$ and ϕ, with values listed in Tables S3 and S4 of the ESI.† These calculations are used to further verify agreement with our proposed $^2J_{Si-O-Si}$ coupling model.

All additional numerical analysis codes were written in python using NumPy libraries.[31] The least square analysis was performed using python's LMFIT[32] module. The graphics were produced using python's matplotlib library.[33]

3 Theory

The J coupling contribution to the nuclear spin Hamiltonian can be written[34]

$$\hat{H}_J = \hat{\mu}_N\cdot\mathscr{K}\cdot\hat{\mu}_{N'} = \hbar^2\gamma_N\gamma_{N'}\hat{\mathbf{I}}_N\cdot\mathscr{K}\cdot\hat{\mathbf{I}}_{N'}. \quad (3)$$

The convention is to combine the gyromagnetic ratio constants and the reduced $\mathscr{K}$ tensor such that

$$\hat{H}_J = \hbar 2\pi\hat{\mathbf{I}}_N\cdot\mathbf{J}\cdot\hat{\mathbf{I}}_{N'}, \quad (4)$$

with

$$\mathbf{J} = \frac{\hbar\gamma_N\gamma_{N'}}{2\pi}\mathscr{K}. \quad (5)$$

This gives a $\mathbf{J}$ tensor with dimensions of inverse time.

As we explored the calculated variations in $^2J_{Si-O-Si}$ with changing cluster structure, we searched for the possible empirical relationships that might characterize the observed correlation of $^2J_{Si-O-Si}$ to structure. In our calculations we found that the majority of the J-coupling arises from the Fermi contact (FC) contribution, and the remaining contributions from spin–dipolar (SD), paramagnetic spin–orbit (PSO), and diamagnetic spin–orbit (DSO), as illustrated in Fig. S2 of the ESI,† account for less than 10% of the net J-coupling. With this in mind, we looked for guidance in the older literature of J coupling theory and focused on the simple and highly approximate MO theory approach outlined by Pople and Santry,[35–40] which considers only the isotropic Fermi contact contribution and yields the expression

$$\mathscr{K}^{(fc)} = \frac{4}{9}\mu_0^2\mu_B^2 s_N^2(0)s_{N'}^2(0)\pi_{N,N'}, \quad (6)$$

where μ_0 is the magnetic constant, μ_B is the Bohr magneton, $s_N(0)$ and $s_{N'}(0)$ are the values of the valence s-orbitals of atoms N and N′ at the nuclei, and $\pi_{N,N'}$ is the mutual atom–atom polarizability of Coulson and Longuet-Higgins,[41] given by

$$\pi_{N,N'} = -4\sum_{i}^{occ}\sum_{j}^{unocc}\frac{c_{\mu,i}c_{\nu,i}c_{\mu,j}c_{\nu,j}}{\varepsilon_j - \varepsilon_i}. \quad (7)$$

Here the summation is over occupied (i) and unoccupied (j) molecular orbitals, $|\psi_i\rangle$, with energy ε_i and given by

$$|\psi_i\rangle = \sum_\mu c_{\mu,i}\left|\phi_\mu\right\rangle, \quad (8)$$

which are expressed in terms of the valence hybrid type orbitals (HTOs), $|\phi_\mu\rangle$, which are given by

$$|\phi_\mu\rangle = a_\mu|s\rangle + (1 - a_\mu^2)^{1/2}|p\rangle, \quad (9)$$

where $|s\rangle$ and $|p\rangle$ are the atomic-type orbitals and a_μ^2 is the s-character of the HTO. In the summation of eqn (7) the μ and ν index the HTOs on N and N′, respectively.

An exhaustive search of the literature reveals few MO theory studies considering the geminal $^2J_{AB}$ coupling between tetrahedrally coordinated atoms. The most relevant and detailed discussion we could find on this topic is a chapter in 1988 by Klessinger and Barfield,[42] examining the dependence of geminal ^{13}C–^{13}C coupling constants. In this case they derive the mutual atom–atom polarizability as

$$\pi_{C_1,C_3} = \frac{a_1^2 a_3^2}{16\beta^3}\left[-4\beta_{2,2'}^2 - \left(\beta_{1',3} - \beta_{2,2'}\right)^2 + \left(\sum_\kappa \beta_{2',\kappa} + \sum_\lambda \beta_{2,\lambda}\right)^2\right] \quad (10)$$

where a_1^2 and a_3^2 are the s-character of the HTOs at carbon C_1 and C_3 along C–C bond directed towards C_2, in a C_1–C_2–C_3 linkage. The integral $\beta_{\mu,\nu}$ is the matrix element of the Hamiltonian operator in the HTO basis set $|\phi_\mu\rangle$,

$$\beta_{\mu,\nu} = \langle\phi_\mu|H|\phi_\nu\rangle. \quad (11)$$

The definition of these integrals are given in Klessinger and Barfield.[42] If all integrals in eqn (10) except $\beta_{2,2'}^2$ are ignored, the mutual atom–atom polarizability term can be approximated[42] to

$$\pi_{C_1,C_3} \propto a_1^2 a_3^2 a_2^4, \quad (12)$$

where a_2^2 is the s-character of the valence HTO at C_2. The $^2J_{C_1,C_3}$ can then be approximated to

$$^2J_{C_1,C_3} \propto a_1^2 a_3^2 a_2^4. \quad (13)$$

While eqn (13) predicts a simple linear correlation of $^2J_{C_1,C_3}$ to the s-character product, we expect this highly approximated correlation to deviate from linearity due to the neglect of the vicinal integrals.[42] Nevertheless, this approximate model provides a useful starting point for developing an empirical expression for geminal J coupling across two coupled ^{29}Si. On the basis of eqn (13), we propose that $^2J_{Si-O-Si}$ is approximately given by

$$^2J_{Si-O-Si} \propto a_{Si_i}^2 a_{Si_j}^2 a_O^4 = \left(a_{Si_i}^2 a_O^2\right)\left(a_{Si_j}^2 a_O^2\right), \quad (14)$$

where $\left(a_{Si_i}^2 a_O^2\right)$ and $\left(a_{Si_j}^2 a_O^2\right)$ are the products of the s-character of the valence HTOs associated with the $Si^{(i)}$–O and $Si^{(j)}$–O bonds across $Si^{(i)}$–O–$Si^{(j)}$ linkage, respectively, as illustrated in Fig. 3.

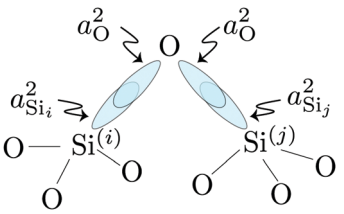

Fig. 3 Simple illustration of valence HTOs associated with the $Si^{(i)}$–O and $Si^{(j)}$–O bonds across $Si^{(i)}$–O–$Si^{(j)}$ linkage.

4 Results and discussion

4.1 Dependence on local structure

In this subsection, we discuss and examine the contributions to the net $^2J_{Si-O-Si}$ coupling arising from the variations in the local structure on the basis of the underlying s-characters a_O^2, $a_{Si_i}^2$, and $a_{Si_j}^2$ at the bridging oxygen and adjacent silicons respectively. These values were determined from the quantum chemistry DFT cluster calculation using Gaussian NBO version 3.1. For clarity, we only present a subset of results from Fig. 2 per structural parameters considered.

Shown in Fig. 4A is the expected dependence of $^2J_{Si-O-Si}$ coupling on $\Omega_0 \in [120^\circ,180^\circ]$, for a subset of results from Fig. 2A where the outer Si–O–Si angles are held constant at $\Omega_{k\neq 0} = 180^\circ$ and the distances held constant at $d_{Si-O} = 1.6$ Å. This dependence of $^2J_{Si-O-Si}$ coupling on the Si–O–Si linkage angle, Ω_0, has been previously discussed by both Cadars *et al.*[26] and Florian *et al.*[25] In Fig. 4B we see the more intriguing result that the $^2J_{Si-O-Si}$ coupling has a markedly linear correlation to the product $a_{Si_i}^2 a_{Si_j}^2 a_O^4$, as predicted by eqn (14). As noted earlier, the slight deviation from linearity observed is not unexpected and is likely attributed to the neglected terms in the mutual atom–atom polarizability term. In Fig. 4C and D we see that the variation in $^2J_{Si-O-Si}$ primarily arises from variation in a_O^4,—the s-character product of the two valence HTOs at the bridging oxygen—while there is a minor yet non-negligible variation coming from $a_{Si_i}^2 a_{Si_j}^2$—the s-character product of the two silicon valence HTOs in the Si–O–Si linkage. The change in a_O^4 is the result of the change in the hybridization of the valence orbitals at the bridging oxygen from sp^2 (33.33% s-character) at $\Omega_0 = 120^\circ$ to sp (50% s-character) at $\Omega_0 = 180^\circ$.

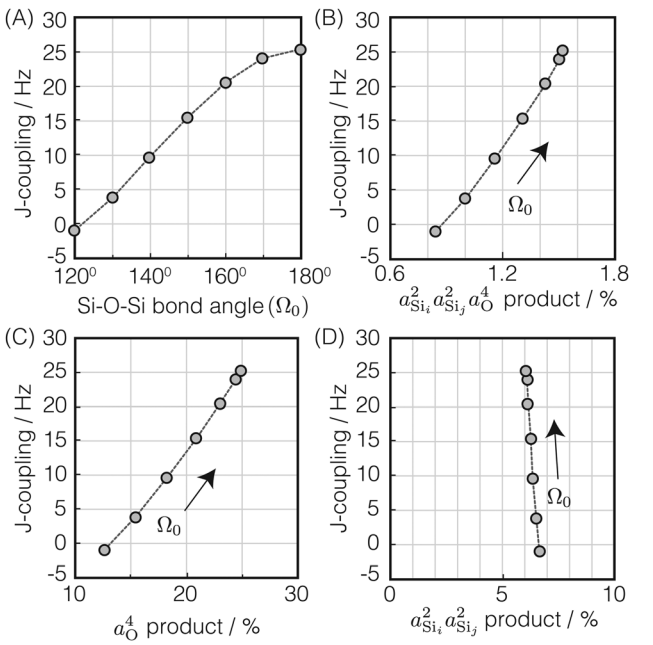

Fig. 4 Dependence of $^2J_{Si-O-Si}$ coupling on (A) Si–O–Si bond angle Ω_0, (B) $a_{Si_i}^2 a_{Si_j}^2 a_O^4$, (C) a_O^4, and (D) $a_{Si_i}^2 a_{Si_j}^2$ for the constraints $\Omega_{k\neq 0} = 180^\circ$ and $d = 1.6$ Å.

A popular approximation for the s-character at the bridging oxygen[9,42] is given by

$$a_{\mathrm{O}}^2 \approx f_{\mathrm{O}}(\Omega) = \frac{\cos\Omega}{\cos\Omega - 1}. \quad (15)$$

Here we use the symbol $f_{\mathrm{O}}(\Omega)$ to distinguish the approximated s-character at the bridging oxygen from the symbol a_{O}^2 for the s-character calculated using quantum chemistry DFT calculations.

With the s-character of each sp^3 valence HTO on a tetrahedral silicon expected to be 25%, the calculated value of $a_{\mathrm{Si}_i}^2 a_{\mathrm{Si}_j}^2$ is also as expected at $\sim(25\%)^2 = 6.25\%$. The slight increase in $a_{\mathrm{Si}_i}^2 a_{\mathrm{Si}_j}^2$ from 6.1% to 6.7% in Fig. 4D with decreasing Ω_0 may seem surprising from a simple hybrid orbital picture—as all intra-tetrahedral angles and Si–O distances are held constant at $\angle$O–Si–O = 109.5° and $d_{\mathrm{Si-O}}$ = 1.6 Å, respectively, in these calculations. In fact, for this subset of results, even the outer Si–O–Si angles are held fixed at 180°, so it is only the variation of the linkage angle Ω_0 that is responsible for this slight change in $a_{\mathrm{Si}_i}^2 a_{\mathrm{Si}_j}^2$. We will examine the origin of this variation shortly when the influence of the outer Si–O–Si angles on $^2J_{\mathrm{Si-O-Si}}$ are considered.

In Fig. 5A is the variation of $^2J_{\mathrm{Si-O-Si}}$ with the two central linkage Si–O bond distances, $d_{\mathrm{Si-O}} \in$ [1.58 Å, 1.62 Å], for a subset of results from Fig. 2C where the central linkage angle was fixed at $\Omega_0 = 180°$ and the outer Si–O–Si angles and outer distances are held constant at $\Omega_{k\neq 0} = 146°$ and $d_{\mathrm{Si-O}}$ = 1.6 Å, respectively. The $^2J_{\mathrm{Si-O-Si}}$ coupling remains relatively constant around 21.5 Hz over this range of central linkage Si–O bond distances, with a slight decrease from ~22 to ~21 Hz with increasing bond length. This relative independence of $^2J_{\mathrm{Si-O-Si}}$ on the central linkage Si–O bond distances is consistent with previous observations by Florian *et al.*[25] In Fig. 5B we find again that the $^2J_{\mathrm{Si-O-Si}}$ coupling has a linear correlation to the product $a_{\mathrm{Si}_i}^2 a_{\mathrm{Si}_j}^2 a_{\mathrm{O}}^4$, and in Fig. 5C we see no observable dependence of $^2J_{\mathrm{Si-O-Si}}$ coupling on the s-character product a_{O}^4 at the bridging oxygen. This is because, for this subset of calculations, the hybridization at the bridging oxygen was locked to sp through the constraint $\Omega_0 = 180°$. Since the s-character at the bridging oxygen predominantly depends on the Si–O–Si bond angle, as noted in eqn (15), the change in Si–O bond distance, $d_{\mathrm{Si-O}}$, shows no observable change in its s-character. In Fig. 5D we find that the minor variation in $^2J_{\mathrm{Si-O-Si}}$ coupling is dominated by the change in $a_{\mathrm{Si}_i}^2 a_{\mathrm{Si}_j}^2$. While a decrease in the a_{Si}^2 with increasing Si–O bond distance has been previously reported by Grimmer and coworkers[10,11] it was in the context of correlated changes in the intra-tetrahedral angle $\angle$O–Si–O. With the intra-tetrahedral angles in this calculation fixed at $\angle$O–Si–O = 109.5°, it seems that changes in Si–O length alone lead to minor variations in a_{Si}^2—although these result in relatively insignificant variations in $^2J_{\mathrm{Si-O-Si}}$.

In Fig. 6A is the variation of $^2J_{\mathrm{Si-O-Si}}$ with the inter-tetrahedral dihedral angle $\phi \in [-60°, 60°]$ for a subset of results from Fig. 2B where the central linkage angle was fixed at $\Omega_0 = 180°$, and the outer Si–O–Si angles and outer distances are held constant at $\Omega_{k\neq 0} = 146°$ and $d_{\mathrm{Si-O}}$ = 1.6 Å, respectively. A periodic modulation of the form $\cos 3\phi$ for $^2J_{\mathrm{Si-O-Si}}$ over a range of 1.6 Hz is observed due to the local three fold symmetry of the $(H_3SiO)_3$–Si–O–Si–$(OSiH_3)_3$ cluster when rotating about ϕ. There is no observable variation in the hybrid orbital s-character products in Fig. 6B–D as expected, since this variation is associated with the vicinal integral terms of the mutual atom–atom polarizability expansion which are completely neglected in eqn (14).

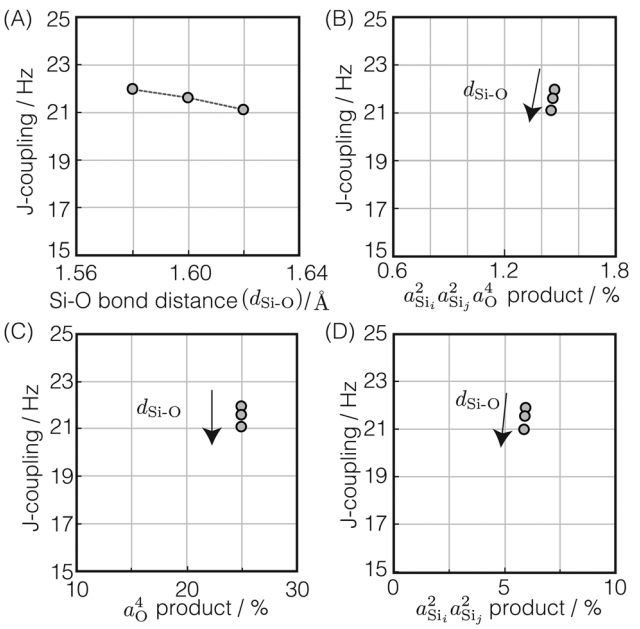

Fig. 5 Dependence of $^2J_{\mathrm{Si-O-Si}}$ coupling on (A) Si–O bond distance, $d_{\mathrm{Si-O}}$, (B) $a_{\mathrm{Si}_i}^2 a_{\mathrm{Si}_j}^2 a_{\mathrm{O}}^4$, (C) a_{O}^4, and (D) $a_{\mathrm{Si}_i}^2 a_{\mathrm{Si}_j}^2$ for the constraints $\Omega_0 = 180°$ and $\Omega_{k\neq 0} = 146°$.

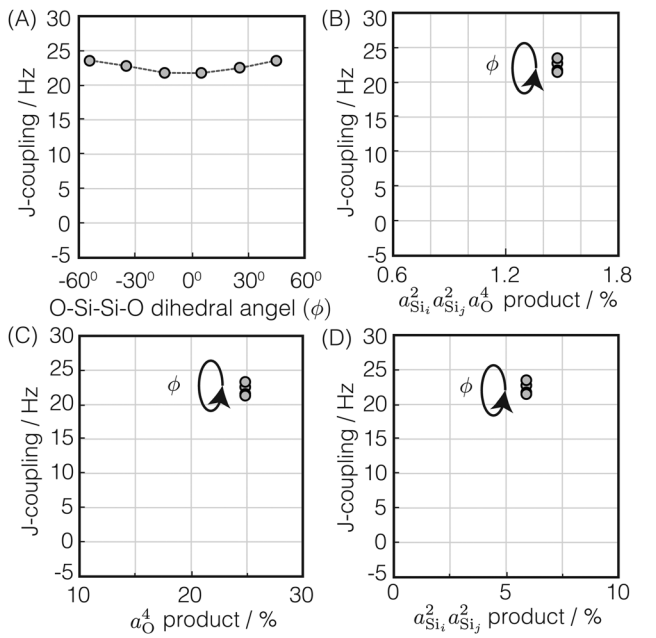

Fig. 6 Dependence of $^2J_{\mathrm{Si-O-Si}}$ coupling on (A) O–Si–Si–O inter tetrahedral dihedral angle, ϕ, (B) $a_{\mathrm{Si}_i}^2 a_{\mathrm{Si}_j}^2 a_{\mathrm{O}}^4$, (C) a_{O}^4, and (D) $a_{\mathrm{Si}_i}^2 a_{\mathrm{Si}_j}^2$ for the constraints $\Omega_{k\neq 0} = 146°$, $\Omega_0 = 180°$ and d = 1.6 Å.

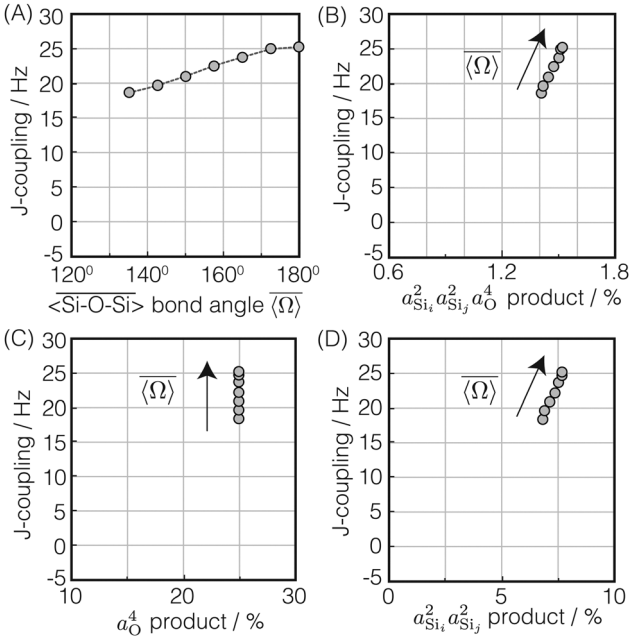

Fig. 7 Dependence of $^2J_{Si-O-Si}$ coupling on (A) the average Si–O–Si bond angles, $\overline{\langle\Omega\rangle}$, (B) $a^2_{Si_i}a^2_{Si_j}a^4_O$, (C) a^4_O, and (D) $a^2_{Si_i}a^2_{Si_j}$ for the constraints $\Omega_0 = 180^\circ$ and $d = 1.6$ Å.

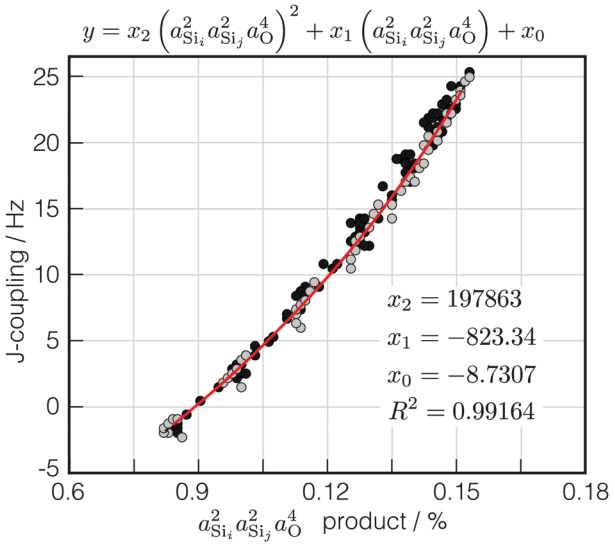

Fig. 8 $^2J_{Si-O-Si}$ coupling as a function of $a^2_{Si_i}a^2_{Si_j}a^4_O$ at $Si^{(i)}$, $Si^{(j)}$ and O across $Si^{(i)}$–O–$Si^{(j)}$ linkage. The points in gray and black corresponds to the systematic ($\Omega_{k\neq0} = \Omega_{out}$) and arbitrary structural variations, respectively.

In Fig. 7A is the variation of $^2J_{Si-O-Si}$ with $\overline{\langle\Omega\rangle}$, as calculated by eqn (2), for a subset of results from Fig. 2A subjected to the constraint $\Omega_0 = 180^\circ$, $\Omega_{k\neq0} = \Omega_{out}$ and $d = 1.6$ Å where Ω_{out} varied from 120° to 180°. The variation in Fig. 7A is about 25% of that shown in Fig. 4A and is found to be the second most dominant dependence of $^2J_{Si-O-Si}$ coupling. As Ω_0 is fixed, it is the change in the outer Si–O–Si bond angles, Ω_{out}, that leads to this variation in $^2J_{Si-O-Si}$. In Fig. 7B we again find the markedly linear correlation of $^2J_{Si-O-Si}$ coupling with $a^2_{Si_i}a^2_{Si_j}a^4_O$ as predicted by eqn (14). As might be expected, no observable dependence of $^2J_{Si-O-Si}$ coupling on a^4_O is observed in Fig. 7C since the hybridization at the bridging oxygen was fixed to sp with the constraint $\Omega_0 = 180^\circ$.

Clearly, the origin of the $^2J_{Si-O-Si}$ dependence on the outer angles, Ω_{out} comes from the variation in $a^2_{Si_i}a^2_{Si_j}$ as seen in Fig. 7D. Why would the $a^2_{Si_i}$ or $a^2_{Si_j}$ increase as the outer angles, Ω_{out}, increase? This is the same question alluded to earlier with respect to Fig. 4D. The logic is as follows. We expect the sum of the s-characters for the four HTO around each silicon to be constant. So, as the s-character of one HTO deviates from 25%, the s-characters of the other HTO compensate to maintain the constant sum. Hence, we expect the s-character of the HTO that is part of the central linkage to increase as the average s-character of the other three HTOs decreases. Close examination of the variation in $a^2_{Si_i}$ as the function of the Si–O–Si tetrahedral angle, Ω_0, and average Si–O–Si bond angle, $\langle\Omega\rangle_i$, also shown in Fig. S3 of the ESI,† reveals an approximate proportionality given by

$$a^2_{Si_i} \propto \cos\Omega_0 - \cos\langle\Omega\rangle_i. \quad (16)$$

In regard to Fig. 4D, since the outer Si–O–Si bond angles are held constant, $\Omega_{k\neq0} = 180^\circ$, the individual s-characters at $Si^{(i)}$ and $Si^{(j)}$ and, therefore, the product, $a^2_{Si_i}a^2_{Si_j}$, decreases as Ω_0 increases.

The highly approximate *J*-coupling model in eqn (14) predicts a linear correlation of $^2J_{Si-O-Si}$ coupling with respect to the s-character product, $a^2_{Si_i}a^2_{Si_j}a^4_O$. From the *ab initio* calculations, shown in Fig. 8, however, we find that the $^2J_{Si-O-Si}$ coupling is better described by a quadratic in the s-character product, $a^2_{Si_i}a^2_{Si_j}a^4_O$, with $R^2 = 0.99164$. As mentioned earlier, this slight curvature is not unexpected, since the model in eqn (14) neglects all the vicinal integrals from the mutual atom–atom polarizability term. Further discussion on the effect of vicinal integrals can be found in the chapter by Klessinger and Barfield.[42]

Fig. 8 shows the $^2J_{Si-O-Si}$ couplings in two different colors, gray and black. The gray dots correspond to couplings evaluated by systematic variation of the local structure, also shown in Fig. 2, and are provided in the Tables S1 and S2 of the ESI.† The black dots correspond to couplings evaluated at arbitrary Ω_k and ϕ and are listed in Tables S3 and S4 of the ESI.† Most notably a consistent trend in $^2J_{Si-O-Si}$ is observed with respect to the s-character product, $a^2_{Si_i}a^2_{Si_j}a^4_O$, for both systematic and arbitrary structural variation.

On the basis of the results and discussion presented here we can now construct an expression relating $^2J_{Si-O-Si}$ to local structure. The most straightforward approach would be a substitution of eqn (15) and (16) into eqn (14). We found, however, that such an approach leads to an excessive number of coefficients for calibrating the relationship. Instead we found that the same relationship can be expressed with fewer coefficients using

$$J\left(\Omega_0, \overline{\langle\Omega\rangle}, \phi\right) \approx -\overline{\langle\Omega\rangle}\cos\Omega_0\left(m_1 f_O^2(\Omega_0) - m_2\cos 3\phi\right) + J_0. \quad (17)$$

For this expression the coefficients $m_1 = 0.778 \pm 0.004$ Hz per °, $m_2 = 0.0058 \pm 0.0005$ Hz per ° and $J_0 = -8.3 \pm 0.1$ Hz were determined by least square minimization of the objective function

$$\arg\min_{J_0} \left|\left| J(ab\ initio) - J(\Omega, \overline{\langle\Omega\rangle}, \phi) \right|\right|_2^2. \quad (18)$$

Note there is a strong cross correlation coefficient $\rho_{m_1,J_0} = -0.918$ between m_1 and J_0 in this determination. A comparison of *ab initio* $^2J_{\text{Si–O–Si}}$ couplings with respect to the $^2J_{\text{Si–O–Si}}$ coupling model in eqn (17) is presented in Fig. 9A. Again, the points in gray and black correspond to systematic and arbitrary variation of the local structure, respectively. Excellent agreement between the $^2J_{\text{Si–O–Si}}$ coupling model and $^2J_{\text{Si–O–Si}}$ coupling from *ab initio* calculation is observed with $R^2 = 0.99518$. Note that in this approach the slight dependence on Si–O bond distance, $d_{\text{Si–O}}$, has been neglected.

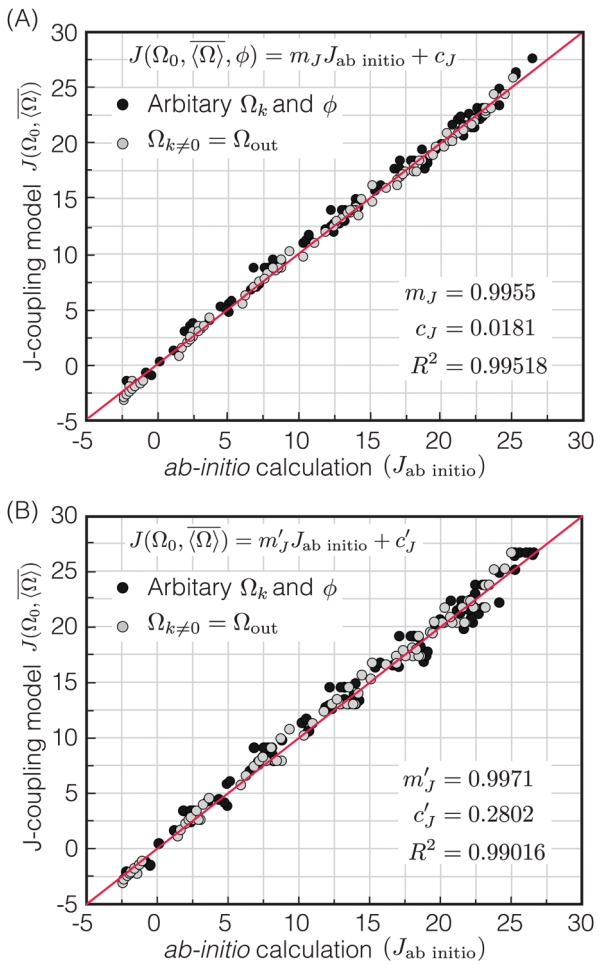

Fig. 9 (A) Plot comparing prediction of $^2J_{\text{Si–O–Si}}$ coupling model, eqn (17), and $^2J_{\text{Si–O–Si}}$ coupling from *ab initio* calculations. Gray and black dots correspond to $^2J_{\text{Si–O–Si}}$ couplings evaluated by systematic and arbitrary structural variations, respectively. The calculated Pearson correlation coefficient is $R^2 = 0.99518$. (B) Plot comparing prediction of $^2J_{\text{Si–O–Si}}$ coupling model, eqn (19) and $^2J_{\text{Si–O–Si}}$ coupling from *ab initio* calculations. The calculated Pearson correlation coefficient is $R^2 = 0.99016$.

Given that $m_2 \ll m_1$ we find that the $^2J_{\text{Si–O–Si}}$ coupling model of eqn (17) can be simplified by dropping the $m_2 \cos 3\phi$ term to obtain

$$J\left(\Omega_0, \overline{\langle\Omega\rangle}\right) \approx -m_1 \overline{\langle\Omega\rangle} \cos\Omega_0 \left(\frac{\cos\Omega_0}{\cos\Omega_0 - 1}\right)^2 + J_0. \quad (19)$$

A comparison of *ab initio* $^2J_{\text{Si–O–Si}}$ couplings with respect to the $^2J_{\text{Si–O–Si}}$ coupling model in eqn (19) is presented in Fig. 9B. Neglecting the ϕ dependence leads to slightly greater scatter which is more noticeable at the higher couplings and a small drop of linear correlation coefficient to $R^2 = 0.99016$. Given this agreement all further analysis will use the $^2J_{\text{Si–O–Si}}$ coupling model of eqn (19).

4.2 Mapping to local structure

Even with our approximate model for $^2J_{\text{Si–O–Si}}$ in eqn (19) being only a function of Ω_0 and $\overline{\langle\Omega\rangle}$ there is no unique mapping of a single $^2J_{\text{Si–O–Si}}$ coupling back to local structure. Fortunately, the ^{29}Si isotropic chemical shift of a Q^4 site has a well established correlation[7,9,43] to the mean inter-tetrahedral angle, $\langle\Omega\rangle$, of a given Q^4, of which, the linear correlation[8]

$$\delta_{\text{CS}} = a_\delta \langle\Omega\rangle + b_\delta, \quad (20)$$

is the simplest, while still giving a reasonably accurate correlation in the relevant range of $\langle\Omega\rangle \in [140°, 160°]$ as detailed further in the ESI.† The data for a number of crystalline silicas and siliceous framework silicates taken from the literature[9,44,45] is shown in Fig. 10, along with a fit to eqn (20) with coefficients a_δ and b_δ provided in Table 1.

The $^2J_{\text{Si–O–Si}}$ coupling across $^{29}\text{Si}^{(i)}$–O–$^{29}\text{Si}^{(j)}$ linkage involves two ^{29}Si isotropic chemical shifts, $\delta_{\text{CS},i}$ and $\delta_{\text{CS},j}$, associated with $^{29}\text{Si}^{(i)}$ and $^{29}\text{Si}^{(j)}$ respectively. Using the linear correlation

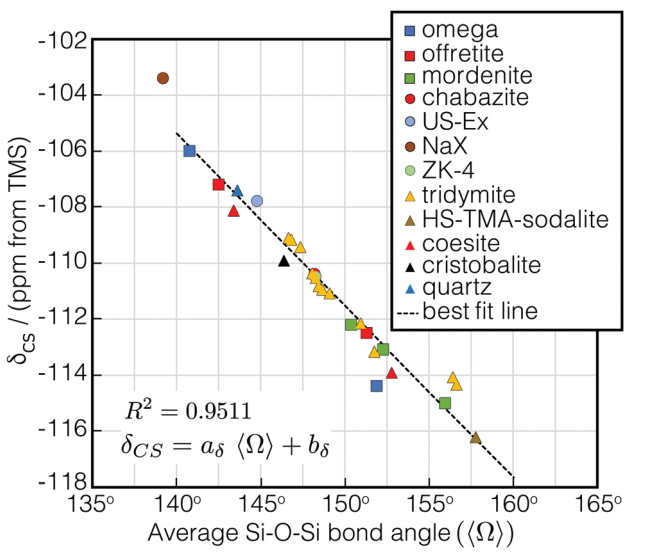

Fig. 10 Linear correlation between average Si–O–Si bond angle, $\langle\Omega\rangle$, about the Si tetrahedron and ^{29}Si isotropic chemical shift, δ_{CS}. Twelve ^{29}Si isotropic chemical shift sites in Tridymite were taken from Kitchin *et al.*[45] and average Si–O–Si bond angles from Baur.[44] The remaining were obtained from Engelhardt and Radeglia[9] and references within.

Table 1 Final coefficients for eqn (22) after calibration with the results of Fig. 10 and eqn (23) after calibration with Sigma-2

Coefficient	Value	Coefficient	Value
a_δ	−0.6148 ppm per °	b_δ	−19.297 ppm
a_j	107.88°	b_j	223.49°
c_j	0.00002487°	d_j	53.01
m_1	0.778 Hz per °	J_0	−7.5 Hz

of eqn (20), the average ^{29}Si isotropic chemical shift is given by

$$\overline{\delta_{CS}} = \frac{1}{2}\left(\delta_{CS,i} + \delta_{CS,j}\right) = a_\delta \overline{\langle\Omega\rangle} + b_\delta. \quad (21)$$

With a simple inversion we have

$$\overline{\langle\Omega\rangle} = \left(\overline{\delta_{CS}} - b_\delta\right)/a_\delta. \quad (22)$$

Inverting eqn (19) for Ω_0 gives

$$\Omega_0 = a_j + b_j\left(\frac{J - J_0}{m_1\overline{\langle\Omega\rangle}}\right) + c_j \exp\left\{d_j\left(\frac{J - J_0}{m_1\overline{\langle\Omega\rangle}}\right)\right\}, \quad (23)$$

where the coefficient a_j, b_j, c_j and d_j are listed in Table 1. Details on the solution for Ω_0 are given in Appendix A. To calibrate eqn (23) against previous experimental measurements we use the ^{29}Si INADEQUATE NMR results of Cadars *et al.*[26] on polycrystalline highly siliceous zeolite Sigma-2, whose structure, shown in Fig. 11A, was predetermined using single crystal X-ray analysis. There are four observable $^2J_{Si–O–Si}$ couplings in Sigma-2. The observed $^2J_{Si–O–Si}$ coupling and the mean ^{29}Si isotropic chemical shift, $\overline{\delta_{CS}}$, of the two coupled nuclei corresponding to the four ^{29}Si–O–^{29}Si pairs from this measurement are listed in Table 2. Here, the mean ^{29}Si isotropic chemical shift, $\overline{\delta_{CS}}$, was determined as half the corresponding ^{29}Si double quantum frequency of the INADEQUATE spectra. The X-ray determined Si–O–Si bond angle, Ω_0 and $\overline{\langle\Omega\rangle}$, for these pairs are also listed in Table 2. We choose to calibrate eqn (23) by only varying J_0 to obtain agreement between model and experiment. This was accomplished by performing a least square minimization of the objective function

$$\arg\min_{J_0} ||\Omega_0(\text{X-ray}) - \Omega_0||_2^2, \quad (24)$$

where Ω_0(X-ray) is the Si–O–Si bond angle inferred from single crystal X-ray analysis, and Ω_0 is the Si–O–Si bond angle calculated using eqn (23) with m_1 = 0.778 Hz per ° held constant. With this approach we obtain best agreement with J_0 = −7.5 ± 0.6 Hz.

A plot of measured $^2J_{Si–O–Si}$ coupling *vs.* $\overline{\delta_{CS}}$ from Sigma-2 is presented in Fig. 11B. Overlaid on top is a grid map of calibrated $\overline{\langle\Omega\rangle}$ and Ω_0. In Fig. 11C, the calculated $\overline{\langle\Omega\rangle}$ and Ω_0 (filled circles) along with X-ray determined $\overline{\langle\Omega\rangle}$ and Ω_0 (open circles) are presented. Overlaid on top is the grid map of J coupling and $\overline{\delta_{CS}}$. Agreement to within ∼3° between Ω_0 from the X-ray and NMR measurements is observed for pairs 4-1, 2-3 and 1-3, while there is a mismatch of ∼7° for the 4-2 pair. With only the limited data from Sigma-2, it is clear that additional experimental efforts in refinement of the calibration of eqn (23) would be helpful. Such efforts are, in fact, currently in progress in our laboratory on highly silicious zeolites using the recently developed PIETA method[46] for rapid and sensitive 2D J NMR spectroscopy.

Overall, the results presented here are extremely promising and open the door to new opportunities to more fully exploit $^2J_{Si–O–Si}$ couplings as quantitative probes of structure in silicates. With only a ∼1 Hz change from the *ab initio* derived value of J_0 = −8.3 ± 0.1 Hz, to the Sigma-2 calibrated value of J_0 = −7.5 ± 0.6 Hz, the proposed correlated models of ^{29}Si chemical shift and $^2J_{Si–O–Si}$ coupling provide an acceptable model for the quantitative interpretation of the $^2J_{Si–O–Si}$ coupling. It will be interesting to see if a similar analysis can be applied with other geminal J couplings across a bridging oxygen, such as a ^{31}P–O–^{31}P or ^{27}Al–O–^{29}Si linkage.

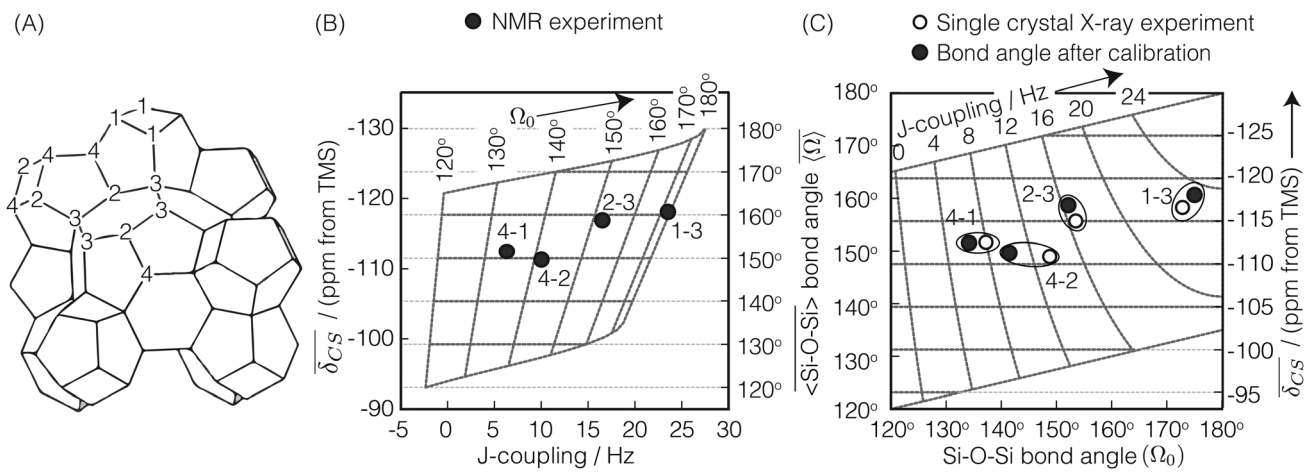

Fig. 11 (A) Schematic of highly siliceous zeolite Sigma-2 adapted from Cadars *et al.*[26] (B) A correlation plot of $\overline{\delta_{CS}}$ and J coupling for Sigma-2 with superimposed calibrated $\overline{\langle\Omega\rangle}$ and Ω_0 grid. (C) Comparison of single crystal X-ray *vs.* NMR determined $\overline{\langle\Omega\rangle}$ and Ω_0 for the four different ^{29}Si pairs in Sigma-2. Superimposed is the $\overline{\delta_{CS}}$ and J coupling grid. A good agreement between the two results is observed for pair 4-1, 2-3 and 1-3.

Table 2 Observed $^2J_{Si-O-Si}$ couplings (column 3) and ^{29}Si average isotropic chemical shift, $\overline{\delta_{CS}}$, (column 2) for the ^{29}Si pairs (column 1) in highly siliceous zeolite Sigma-2.[26] Listed along column 4 and 5, is Ω_0 and $\overline{\langle\Omega\rangle}$ obtained from the crystal structure determined by single crystal X-ray analysis. Listed in column 6 and 7, is the Ω_0 and $\overline{\langle\Omega\rangle}$ calculated using eqn (22) and (23)

	Experimental		Calculated			
	NMR		*Via* X-ray		*Via* NMR	
^{29}Si pair	$\overline{\delta_{CS}}$/ppm	J/Hz	Ω_0/°	$\overline{\langle\Omega\rangle}$/°	Ω_0/°	$\overline{\langle\Omega\rangle}$/°
1-3	−118.0	23.5	172.8	158.2	176.0	160.5
2-3	−116.8	16.5	153.5	155.6	152.0	158.6
4-2	−111.25	10.0	148.7	148.9	141.5	149.5
4-1	−112.4	6.3	137.2	151.6	134.0	151.4

5 Summary

While both scalar *J*-couplings and homonuclear dipolar coupling are used qualitatively to establish connectivities between Si sites, it has been primarily homonuclear ^{29}Si–^{29}Si dipolar couplings through measurements of double quantum buildup curves that have provided some of the most useful quantitative details in the structure refinement of many siliceous zeolites and NMR crystallographic structural studies of meso- and microporous silicate materials.[18,47,48] Here we have examined whether $^2J_{Si-O-Si}$, the geminal coupling across a Si–O–Si linkage, can be turned into a more quantitative probe of the local structure in silicate networks.

Using high level density function theory (DFT) methods, we have found that the two main influences on the $^2J_{Si-O-Si}$ couplings are a primary dependence on the linkage Si–O–Si angle and a secondary dependence on mean Si–O–Si linkage of the two coupled ^{29}Si nuclei. We show that the simple and highly approximate MO theory approach outlined by Pople and Santry[35–40] can provide key insights when developing approximate models for geminal *J*-couplings based on results from high level density function theory (DFT) methods.[25,26] Exploiting a well established correlation between ^{29}Si isotropic chemical shift and the mean Si–O–Si angle of a Q^4 site, we have developed an approach where a correlation plot of $^2J_{Si-O-Si}$ to mean ^{29}Si isotropic chemical shift can be mapped into a 2D correlation of linkage Si–O–Si bond angle, Ω_0, to mean Si–O–Si bond angle of the two coupled ^{29}Si. Using available experimental $^2J_{Si-O-Si}$ couplings from Sigma-2,[26] we found that only a minor adjustment of one *ab initio* derived coefficient in our $^2J_{Si-O-Si}$ model was needed to bring our model in line with experimental results.

Conflicts of interest

There are no conflicts to declare.

Appendix

A Inversion of $^2J_{Si-O-Si}$ to Ω_0

For inversion of eqn (19) with respect to Ω_0, a close form solution can be obtained by first recasting eqn (19) into the form of a cubic equation

$$\lambda^3 + x\lambda^2 - \frac{x}{2}\lambda + x = 0, \tag{25}$$

where $\lambda = \cos\Omega_0$, and

$$x = \frac{J - J_0}{m_1\overline{\langle\Omega\rangle}}. \tag{26}$$

The roots of eqn (25) are

$$\lambda_1(x) = -\frac{1}{3}x + [S(x) + T(x)], \tag{27a}$$

$$\lambda_2(x) = -\frac{1}{3}x - \frac{1}{2}[S(x) + T(x)] + i\frac{1}{2}\sqrt{3}[S(x) - T(x)], \tag{27b}$$

$$\lambda_3(x) = -\frac{1}{3}x - \frac{1}{2}[S(x) + T(x)] - i\frac{1}{2}\sqrt{3}[S(x) - T(x)], \tag{27c}$$

where we have defined

$$T(x) = \sqrt[3]{R(x) - \sqrt{D(x)}}, \tag{28a}$$

$$S(x) = \sqrt[3]{R(x) + \sqrt{D(x)}}, \tag{28b}$$

$$R(x) = -\frac{1}{54}x(2x^2 + 18x + 27), \tag{28c}$$

$$D(x) = \frac{1}{108}x^2(4x + 27). \tag{28d}$$

The number of real and complex roots can be determined from the sign of the discriminant, $D(x)$ in eqn (28d):

- If $D(x) > 0$, one root is real and two are complex conjugate.
- If $D(x) = 0$, all roots are real with at least two equal.
- If $D(x) < 0$, all roots are real and unequal.

For the given problem, the discriminant $D(x)$, eqn (28d), is positive if $x > -6.75$. For given $J_0 < 0$ Hz and $m_1 > 0°\ \text{Hz}^{-1}$, x is always positive and so is the discriminant. Therefore, there exists only one real root of eqn (25) given by eqn (27a). Thus, the inversion of eqn (19) with respect to Ω_0 is

$$\Omega_0(x) = \frac{180^\circ}{\pi}\cos^{-1}[\lambda_1(x)]. \tag{29}$$

To further simplify this result, $\Omega_0(x)$ was approximated to a function $g(x)$ that closely resembles $\Omega_0(x)$ within the relevant range of 120° to 180°. For $\Omega_0(x) \in [120°,180°]$, $\lambda_1(x)$ maps to a range $\lambda_1(x) \in [-0.5, -1.0]$ which further maps to a range $x \in [1/18,1/4]$. Within the relevant range $x \in [1/18,1/4]$, $\Omega_0(x)$ can be approximated as

$$g(x) = a_j + b_j\,x + c_j\exp\{d_j\,x\}, \tag{30}$$

where the coefficients are listed in Table 1. The function $g(x)$ provides a good approximation of $\Omega_0(x)$ with $|g(x) - \Omega_0(x)| < 0.5°$ within the range $\Omega_0(x) \in [120°, 176°]$. Deviations from 176° and onwards to a maximum of 3.7° at $\Omega_0(x) = 180°$ is significant although can be neglected because of its low probability. A comparison of $\Omega_0(x)$ and $g(x)$ as a function of x is provided in the ESI.†

Acknowledgements

This material is based upon work supported by the National Science Foundation under Grant No. CHE-1506870.

References

1 G. Engelhardt and D. Michel, *High-resolution solid-state NMR of silicates and zeolites*, John Wiley & Sons, Chichester, 1987.
2 C. A. Fyfe, *Solid-State NMR for Chemists*, C.F.C. Press, Guelph, 1983.
3 K. J. D. Mackenzie and M. E. Smith, *Multinuclear Solid-State NMR of Inorganic Materials*, Pergamon, 2002.
4 N. Janes and E. Oldfield, *J. Am. Chem. Soc.*, 1985, **107**, 6769–6775.
5 J. F. Stebbins and B. T. Poe, *Geophys. Res. Lett.*, 1999, **26**, 2521–2523.
6 G. Engelhardt, H. Jancke, D. Hoebbel and W. Wieker, *Z. Chem.*, 1974, **14**, 109–110.
7 J. V. Smith and C. S. Blackwell, *Nature*, 1983, **303**, 223–225.
8 J. Thomas, J. Klinowski, S. Ramdas, B. Hunter and D. Tennakoon, *Chem. Phys. Lett.*, 1983, **102**, 158–162.
9 G. Engelhardt and R. Radeglia, *Chem. Phys. Lett.*, 1984, **108**, 271–274.
10 A.-R. Grimmer, E. F. Gechner and G. Molgedey, *Chem. Phys. Lett.*, 1981, **77**, 331–335.
11 A.-R. Grimmer, *Chem. Phys. Lett.*, 1985, **119**, 416–420.
12 J. F. Stebbins, *Nature*, 1987, **330**, 465.
13 P. Zhang, C. Dunlap, P. Florian, P. J. Grandinetti, I. Farnan and J. F. Stebbins, *J. Non-Cryst. Solids*, 1996, **204**, 294–300.
14 P. Zhang, P. J. Grandinetti and J. F. Stebbins, *J. Phys. Chem. B*, 1997, **101**, 4004–4008.
15 M. Davis, D. C. Kaseman, S. M. Parvani, K. J. Sanders, P. J. Grandinetti, P. Florian and D. Massiot, *J. Phys. Chem. A*, 2010, **114**, 5503–5508.
16 M. Davis, K. J. Sanders, P. J. Grandinetti, S. J. Gaudio and S. Sen, *J. Non-Cryst. Solids*, 2011, **357**, 2787–2795.
17 J. H. Baltisberger, P. Florian, E. G. Keeler, P. A. Phyo, K. J. Sanders and P. J. Grandinetti, *J. Magn. Reson.*, 2016, **268**, 95–106.
18 D. H. Brouwer, *J. Am. Chem. Soc.*, 2008, **130**, 6306–6307.
19 R. K. Harris and C. T. G. Knight, *J. Chem. Soc., Faraday Trans. 2*, 1983, **79**, 1525–1538.
20 R. K. Harris and C. T. G. Knight, *J. Chem. Soc., Faraday Trans. 2*, 1983, **79**, 1539–1561.
21 R. K. Harris, M. J. O'Connor, E. H. Curzon and O. W. Howarth, *J. Magn. Reson.*, 1984, **57**, 115–122.
22 M. Haouas and F. Taulelle, *J. Phys. Chem. B*, 2006, **110**, 3007–3014.
23 H. Cho, A. R. Felmy, R. Craciun, J. P. Keenum, N. Shah and D. A. Dixon, *J. Am. Chem. Soc.*, 2006, **128**, 2324–2335.
24 S. Cadars, A. Lesage, N. Hedin, B. F. Chmelka and L. Emsley, *J. Phys. Chem. B*, 2006, **110**, 16982–16991.
25 P. Florian, F. Fayon and D. Massiot, *J. Phys. Chem. C*, 2009, **113**, 2562–2572.
26 S. Cadars, D. H. Brouwer and B. F. Chmelka, *Phys. Chem. Chem. Phys.*, 2009, **11**, 1825–1837.
27 J. Autschbach and B. Le Guennic, *J. Chem. Educ.*, 2007, **84**, 156.
28 M. J. Frisch, G. W. Trucks, H. B. Schlegel, G. E. Scuseria, M. A. Robb, J. R. Cheeseman, G. Scalmani, V. Barone, B. Mennucci, G. A. Petersson, H. Nakatsuji, M. Caricato, X. Li, H. P. Hratchian, A. F. Izmaylov, J. Bloino, G. Zheng, J. L. Sonnenberg, M. Hada, M. Ehara, K. Toyota, R. Fukuda, J. Hasegawa, M. Ishida, T. Nakajima, Y. Honda, O. Kitao, H. Nakai, T. Vreven, J. A. M. Jr., J. E. Peralta, F. Ogliaro, M. J. Bearpark, J. J. Heyd, E. N. Brothers, K. N. Kudin, V. N. Staroverov, T. A. Keith, R. Kobayashi, J. Normand, K. Raghavachari, A. P. Rendell, J. C. Burant, S. S. Iyengar, J. Tomasi, M. Cossi, N. Rega, J. M. Millam, M. Klene, J. E. Knox, J. B. Cross, V. Bakken, C. Adamo, J. Jaramillo, R. Gomperts, R. E. Stratmann, O. Yazyev, A. J. Austin, R. Cammi, C. Pomelli, J. W. Ochterski, R. L. Martin, K. Morokuma, V. G. Zakrzewski, G. A. Voth, P. Salvador, J. J. Dannenberg, S. Dapprich, A. D. Daniels, O. Farkas, J. B. Foresman, J. V. Ortiz, J. Cioslowski and D. J. Fox, *Gaussian 09 Revision D.01*, 2013.
29 O. S. Center, *Ohio Supercomputer Center*, 1987.
30 E. D. Glendening, A. E. Reed, J. E. Carpenter and F. Weinhold, *NBO Version3.1*, 1988.
31 S. van der Walt, S. C. Colbert and G. Varoquaux, *Comput. Sci. Eng.*, 2011, **13**, 22–30.
32 M. Newville, T. Stensitzki, D. B. Allen and A. Ingargiola, *LMFIT: Non-Linear Least-Square Minimization and Curve-Fitting for Python*, 2014.
33 J. D. Hunter, *Comput. Sci. Eng.*, 2007, **9**, 90–95.
34 P. J. Grandinetti, J. T. Ash and N. M. Trease, *Prog. Nucl. Magn. Reson. Spectrosc.*, 2011, **59**, 121–196.
35 J. Pople and D. Santry, *Mol. Phys.*, 1964, **7**, 269–286.
36 J. Pople and D. Santry, *Mol. Phys.*, 1964, **8**, 1–18.
37 J. Pople and D. Santry, *Mol. Physiol.*, 1965, **9**, 311–318.
38 J. Pople and D. Santry, *Mol. Phys.*, 1965, **9**, 301–310.
39 J. A. Pople, D. P. Santry and G. A. Segal, *J. Chem. Phys.*, 1965, **43**, S129–S135.
40 M. Barfield, *Magn. Reson. Chem.*, 2007, **45**, 634–646.
41 C. A. Coulson and H. C. Longuet-Higgins, *Proc. R. Soc. London, Ser. A*, 1947, **191**, 39–60.
42 M. Klessinger and M. Barfield, *The structural dependence of geminal 13C–13C coupling constants*, Ellis Horwood, Chichester, 1987, ch. 16, pp. 269–284.
43 F. Mauri, A. Pasquarello, B. G. Pfrommer, Y.-G. Yoon and S. G. Louie, *Phys. Rev. B: Condens. Matter Mater. Phys.*, 2000, **62**, 4786–4789.
44 W. H. Baur, *Acta Crystallogr., Sect. B: Struct. Crystallogr. Cryst. Chem.*, 1977, **33**, 2615–2619.
45 S. J. Kitchin, S. C. Kohn, R. Dupree, C. M. B. Henderson and K. Kihara, *Am. Mineral.*, 1996, **81**, 550–560.
46 J. H. Baltisberger, B. J. Walder, E. G. Keeler, D. C. Kaseman, K. J. Sanders and P. J. Grandinetti, *J. Chem. Phys.*, 2012, **136**, 211104.
47 D. H. Brouwer, S. Cadars, J. Eckert, Z. Liu, O. Terasaki and B. F. Chmelka, *J. Am. Chem. Soc.*, 2013, **135**, 5641–5655.
48 D. H. Brouwer, *Solid-State NMR Spectrosc.*, 2013, **51–52**, 37–45.

Supplementary Information: Correlating geminal $^2J_{\text{Si-O-Si}}$ couplings to structure in framework silicates.

D. J. Srivastava[a], P. Florian[b], J. H. Baltisberger[c] and P. J. Grandinetti*[a1]

[a] *Department of Chemistry and Biochemistry, 100 West 18th Avenue, Columbus, OH, USA. E-mail: grandinetti.1@osu.edu*

[b] *CNRS, UPR3079 CEMHTI, 1D Avenue de la Recherche Scientifique, 45071 Orléans Cedex 2, France.*

[c] *Division of Natural Science, Mathematics, and Nursing, Berea College, Berea, KY, USA.*

S1. GAUSSIAN INTEGRATION GRID SIZE

The effect of change in $^2J_{\text{Si-O-Si}}$ coupling evaluation with the size of the integration grid was tested to avoid integration errors. A series of calculations were run with (*1*) *'fine'*, pruned (75, 302) and (*2*) *'ultrafine'*, pruned (99, 590) integration grids. As seen in Fig. S1, no difference in the $^2J_{\text{Si-O-Si}}$ coupling was observed with the increase in the integration grid size. Thus, all remaining calculations were run with *'fine'* integration grid.

S2. CONTRIBUTIONS TO THE NET J COUPLING

The net J-coupling includes contributions from Fermi contact (FC), Spin-dipolar (SD), paramagnetic spin-orbit (PSO) and diamagnetic spin-orbit (DSO).

$$J = J_{\text{FC}} + J_{\text{SD}} + J_{\text{PSO}} + J_{\text{DSO}}$$

For $^2J_{\text{Si-O-Si}}$ couplings—calculated using Gaussian 09[1] with high level of theory—across a Si-O-Si linkage, the net J-coupling is dominated by the Fermi contact term. As shown in Fig. S2, the combined contribution from SD, PSO, DSO terms account to less than 10% of the contribution from net J-coupling. The combined contribution increases slightly around indexes 1 to 10, indexes 52-67 and indexes 108, 114, 120 and 126, and is associated with clusters with lower Si-O-Si bond angles, Ω_0 in the range of 120° to 130°.

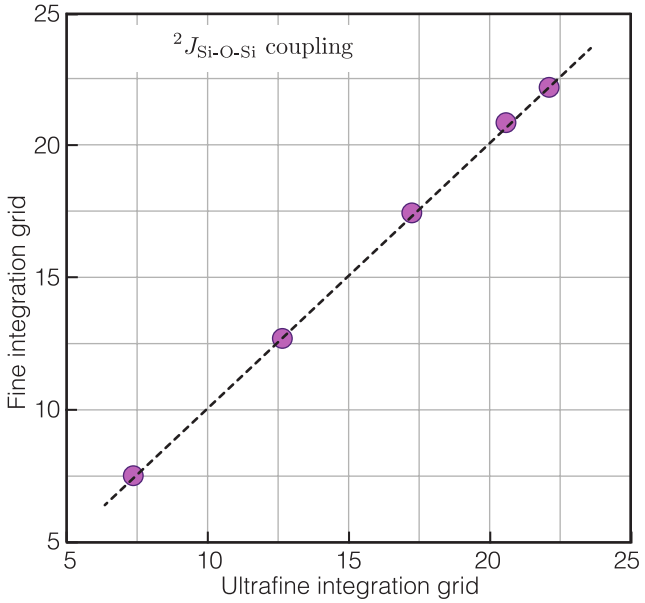

FIG. S1. A perfect correlation of $^2J_{\text{Si-O-Si}}$ coupling evaluated from *'fine'* and *'ultrafine'* integration grid.

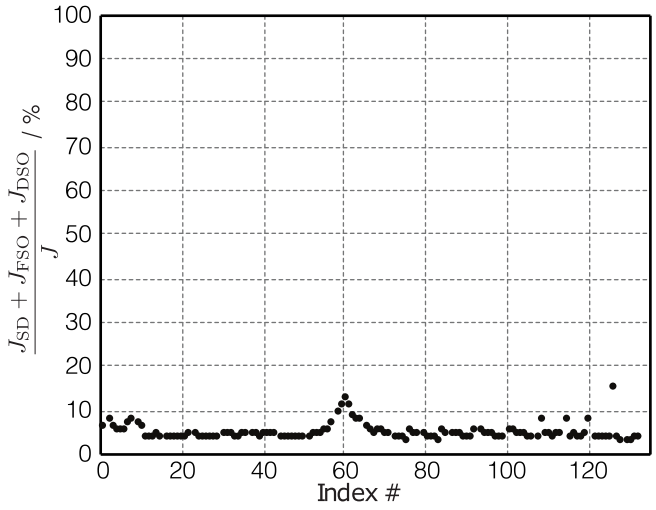

FIG. S2. Combined contribution from SD, PSO and DSO terms accounts to less that 10% of the net J-coupling. The horizontal axis—labeled as index—refer to the index number in Table S1-S3.

S3. S-CHARACTER MODEL

A. s-character at the Si HTO along Si-O bond

In cluster calculations with all the Si-O bond distances fixed at $d_{\text{Si-O}} = 1.6$ Å and with all intra-tetrahedral-angles fixed at $\angle$O-Si-O = 109.5°, we found that the a^2_{Si} of a given Si-O bond depends not only on the Si-O-Si bond angle of its linkage, but also on the other three Si-O-Si bond angles around the silicon. As explained in the main text this arises because the sum of a^2_{Si} from all four Si-O bonds about the Si tetrahedron must remain constant. A strong correlation between a^2_{Si} of a given Si-O bond and the four surrounding Si-O-Si bond angles was found to be

$$a^2_{\text{Si}} \approx c_{\text{Si}} + m_{\text{Si}} \left(\cos\Omega_0 - \cos\langle\Omega\rangle\right), \qquad (1)$$

where $m_{\text{Si}} = 0.0279$, $c_{\text{Si}} = 0.2465$ with $R^2 = 0.96894$. The *ab-initio*-derived data supporting this correlation are

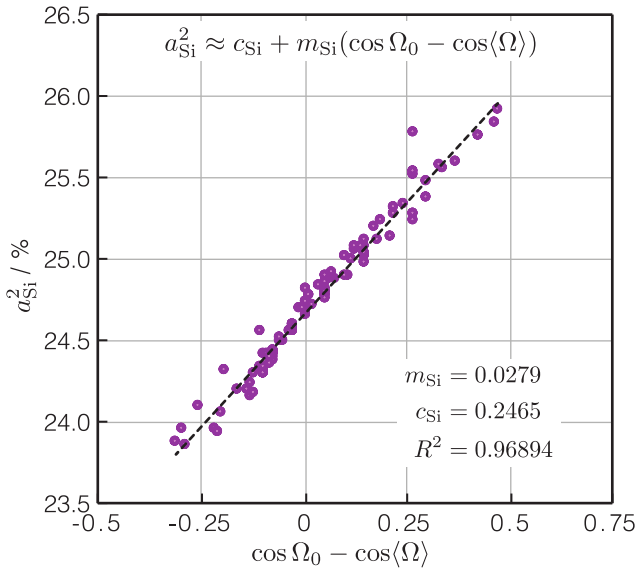

FIG. S3. Variation in the s-character at Si HTO along the Si-O bond as the function of the Si-O-Si tetrahedral angle Ω_0 and average Si-O-Si bond angle, $\langle\Omega\rangle$.

shown in Fig. S3. From Eq. (1), it follows that when all four Si-O-Si bond angles about the Si tetrahedron are equal, the s-character along all four Si-O bonds are also equal.

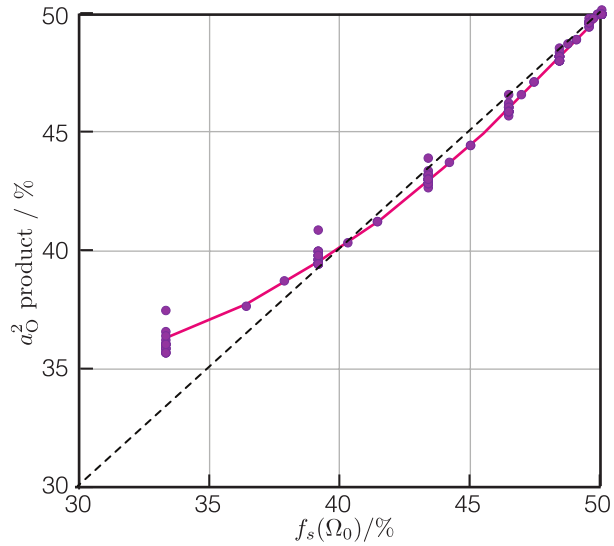

FIG. S4. Comparison of the s-character at bridging oxygen HTO along the Si-O bond against the popular[2,3] approximation $f_s(\Omega_0)$.

B. s-character at the bridging O HTO along Si-O bond

The popular[2,3] approximation of the s-character at the bridging oxygen along the Si-O bond follows,

$$f_s(\Omega_0) = \frac{\cos\Omega_0}{\cos\Omega_0 - 1}. \tag{2}$$

Although the approximation in Eq. (2) gives a good agreement with respect to *ab-initio* calculated s-character, $a^2_{\rm O}$, at higher Ω_0, we shown in Fig. S4 that this agreement appears to break at lower Ω_0.

S4. ^{29}SI ISOTROPIC CHEMICAL SHIFT

In 1983, Smith and Blackwell[4] first showed a correlation between the ^{29}Si isotropic chemical shift, δ_{CS}, and the average secant of the four Si-O-Si bond angles, Ω, about a Si tetrahedron given by

$$\delta_{CS} = a'_\delta\ \langle\sec\Omega\rangle + b'_\delta. \tag{3}$$

Later, the same year, Thomas *et. al.*[5] showed that ^{29}Si isotropic chemical shift correlate linearly with $\langle\Omega\rangle$, according to

$$\delta_{CS} = a_\delta\ \langle\Omega\rangle + b_\delta. \tag{4}$$

The two models, stating different apparent correlations, both showed a good agreement with experiment. In 1984, Engelhardt and Radeglia[3], with the assumption that the chemical shift is dominated by paramagnetic contribution, described ^{29}Si isotropic chemical shift using a simple quantum mechanical model to follow

$$\delta_{CS} = A_\delta \sum_{n=1}^{4} f_{\rm O}(\Omega_n) + B_\delta. \tag{5}$$

The authors showed that the reason Eqs. (3)-(5) all show a good agreement with experiment is that the weak curvature of both $f_{\rm O}(\Omega)$ and $\sec\Omega$ in the relevant range of about 140°-160° cause the ^{29}Si isotropic chemical shift to remain mostly linear with respect to the average Si-O-Si bond angle, $\langle\Omega\rangle$. Many other models[6] have since been proposed, however, by far the simplest correlation is given by Thomas *et. al.*[5], which can be derived by performing a Taylor series expansion of Eq. (5) about 150° with coefficients

$$a_\delta = 1.0025 \times 10^{-2} A_\delta \text{ and } b_\delta = 0.3527\ A_\delta + B_\delta.$$

The coefficient $A_\delta = -61.7625$ ppm/° and $B_\delta = 2.19$ ppm from Engelhardt and Radeglia[3] yields $a_\delta = -0.6191$ ppm/° and $b_\delta = -19.593$ ppm which is within 1.5% of the linear fit reported in the main document.

S5. J-COUPLING AS A FUNCTION OF Ω_0

Cadars *et. al.*[7] discussed the scattering of $^2J_{\text{Si-O-Si}}$ coupling as a function of the central linkage angle Ω_0 resulting from the local structural variations about the central

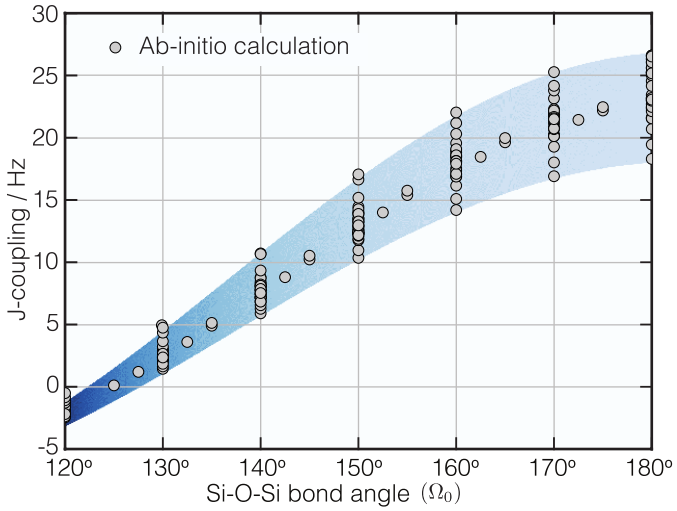

FIG. S5. Scattering of ^2J-coupling as a function of central Si-O-Si linkage angle Ω_0 arising from the variation is local structure around the central Si-O-Si linkage, specially the double average $\overline{\langle\Omega\rangle}$. The gray dots are the *ab-initio* calculated ^2J-couplings and the background image is the intensity plot of ^2J-coupling assuming a uniform distribution of $\overline{\langle\Omega\rangle}$.

Si-O-Si linkage. In Fig. S5 we show the extent of this scattering as a function of Ω_0. The gray dots are the *ab-initio* calculated J-couplings—presented in Table S1-S4—and the image in the background is calculated using Eq. (19) from the main document—assuming a uniform distribution of $\overline{\langle\Omega\rangle}$. A significant scatter of J-coupling is observed when only considering the center linkage angle Ω_0—specially at higher Ω_0.

S6. J-COUPLING MODEL APPROXIMATION

In the main text, we described an analytical expression for calculating the Si-O-Si bond angle

$$\Omega_0(x) = \frac{180^\circ}{\pi}\cos^{-1}\left[-\frac{1}{3}x + \{S(x)+T(x)\}\right], \qquad (6)$$

where

$$\begin{aligned} S(x) &= \sqrt[3]{R(x)+\sqrt{D(x)}},\\ T(x) &= \sqrt[3]{R(x)-\sqrt{D(x)}},\\ D(x) &= \frac{1}{108}x^2\left(4x+27\right),\\ R(x) &= -\frac{1}{54}x\left(2x^2+18x+27\right) \text{ and}\\ x &= \frac{J-J_0}{m_1\overline{\langle\Omega\rangle}}. \end{aligned}$$

Due to the overly complicated parameterization of Eq. (6), we approximated Eq. (6) by

$$g(x) = a_j + b_j\ x + c_j\ \exp\{d_j\ x\} \qquad (8)$$

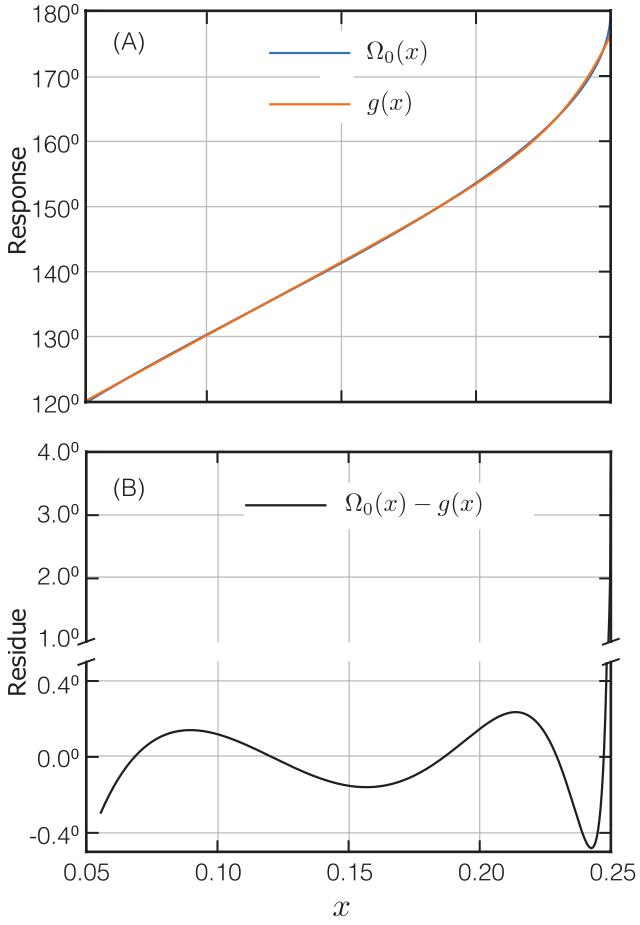

FIG. S6. (A) Comparison of $\Omega_0(x)$ and $g(x)$ as a function of $x \in [1/18, 1/4]$. A good agreement between $g(x)$ and $\Omega_0(x)$ is observed within the range corresponding to $\Omega_0 \in [120°, 176°]$ shown in (B).

where the coefficients $a_j = 107.88°$, $b_j = 223.49°$, $c_j = 0.00002487°$ and $d_j = 53.01$ were determined from the least square minimization. In Fig. S6, we show the comparison between $\Omega_0(x)$ and $g(x)$. A good agreement is observed for the range of x corresponding to $\Omega_0(x) \in [120°, 176°]$ to within $\pm 0.5°$. The deviation at 176° and onwards is significant to a maximum of 3.7° at $\Omega_0(x) = 180°$. However, due to the low probability of Si-O-Si bond angles in this range $[176°, 180°]$, this deviation has been neglected in our study.

[1] M. J. Frisch, G. W. Trucks, H. B. Schlegel, G. E. Scuseria, M. A. Robb, J. R. Cheeseman, G. Scalmani, V. Barone, B. Mennucci, G. A. Petersson, H. Nakatsuji, M. Caricato, X. Li, H. P. Hratchian, A. F. Izmaylov, J. Bloino, G. Zheng, J. L. Sonnenberg, M. Hada, M. Ehara, K. Toyota, R. Fukuda, J. Hasegawa, M. Ishida, T. Nakajima, Y. Honda, O. Kitao, H. Nakai, T. Vreven, J. A. M. Jr., J. E. Peralta, F. Ogliaro, M. J. Bearpark, J. J. Heyd, E. N. Brothers, K. N. Kudin, V. N. Staroverov, T. A. Keith, R. Kobayashi, J. Normand, K. Raghavachari, A. P. Rendell, J. C. Burant, S. S. Iyengar, J. Tomasi, M. Cossi, N. Rega, J. M. Millam, M. Klene, J. E. Knox, J. B. Cross, V. Bakken, C. Adamo, J. Jaramillo, R. Gomperts, R. E. Stratmann, O. Yazyev, A. J. Austin, R. Cammi, C. Pomelli, J. W. Ochterski, R. L. Martin, K. Morokuma, V. G. Zakrzewski, G. A. Voth, P. Salvador, J. J. Dannenberg, S. Dapprich, A. D. Daniels,

O. Farkas, J. B. Foresman, J. V. Ortiz, J. Cioslowski, D. J. Fox, Gaussian 09 Revision D.01 (2013).

[2]M. Klessigner, M. Barfield, The structural dependence of geminal ^{13}C–^{13}C coupling constants, Ellis Horwood, Chichester, 1987, Ch. 16, pp. 269–284.

[3]G. Engelhardt, R. Radeglia, A semi-empirical quantum-chemical rationalization of the correlation between SiOSi angles and ^{29}Si NMR chemical shifts of silica polymorphs and framework aluminosilicates (zeolites), Chemical Physics Letters 108 (1984) 271 – 274. doi:10.1016/0009-2614(84)87063-3.

[4]J. V. Smith, C. S. Blackwell, Nuclear magnetic resonance of silica polymorphs, Nature 303 (1983) 223 – 225. doi:10.1038/303223a0.

[5]J. Thomas, J. Klinowski, S. Ramdas, B. Hunter, D. Tennakoon, The evaluation of non-equivalent tetrahedral sites from ^{29}Si NMR chemical shifts in zeolites and related aluminosilicates, Chemical Physics Letters 102 (1983) 158 – 162. doi:10.1016/0009-2614(83)87384-9.

[6]F. Mauri, A. Pasquarello, B. G. Pfrommer, Y.-G. Yoon, S. G. Louie, Si-O-Si bond-angle distribution in vitreous silica from first-principles ^{29}Si NMR analysis, Phys. Rev. B 62 (8) (2000) 4786–4789.

[7]S. Cadars, D. H. Brouwer, B. F. Chmelka, Probing local structures of siliceous zeolite frameworks by solid-state NMR and first-principles calculations of ^{29}Si-O-^{29}Si scalar couplings, Phys. Chem. Chem. Phys. 11 (2009) 1825–1837. doi:10.1039/b815361b.

TABLE S1. *ab-initio* calculated vs $^2J_{\text{Si-O-Si}}$ coupling model $J(\Omega_0, \overline{\langle\Omega\rangle}, \phi)$ and $J(\Omega_0, \overline{\langle\Omega\rangle})$, Eq. (17) and (19) respectively of the main document, as a function of local parameters including Ω, $\overline{\langle\Omega\rangle}$ and ϕ. The initial geometry was optimized with RHF/6-311G(d). Individual geometry, after structural constraint on Ω_0, Ω_k and ϕ, was not optimized. All Si-O bond distances were fixed to 1.6 Å and O-Si-O intra-tetrahedral angle set to 109.5°.

Index	$\Omega_0/1^\circ$	$\Omega_k/1^\circ$						$\overline{\langle\Omega\rangle}/1^\circ$	$\phi/1^\circ$	$^2J_{\text{Si-O-Si}}$-coupling /Hz		
		Ω_1	Ω_2	Ω_3	Ω_4	Ω_5	Ω_6			*ab-initio*	$J(\Omega_0, \overline{\langle\Omega\rangle}, \phi)$	$J(\Omega_0, \overline{\langle\Omega\rangle})$
1	120	146	146	146	146	146	146	139.5	-59.837	-1.8738	-1.7949	-2.1819
2	120	146	146	146	146	146	146	139.5	-45.539	-1.4292	-1.9006	-2.1819
3	120	146	146	146	146	146	146	139.5	-20.286	-1.8025	-2.3703	-2.1819
4	120	146	146	146	146	146	146	139.5	8.237	-1.9657	-2.5334	-2.1819
5	120	146	146	146	146	146	146	139.5	36.126	-1.9524	-2.0598	-2.1819
6	130	146	146	146	146	146	146	142	-42.783	3.0394	2.9474	2.6332
7	130	146	146	146	146	146	146	142	-18.639	2.4312	2.3494	2.6332
8	130	146	146	146	146	146	146	142	7.502	2.2193	2.1653	2.6332
9	130	146	146	146	146	146	146	142	33.269	2.4992	2.7195	2.6332
10	130	146	146	146	146	146	146	142	56.619	2.9022	3.1317	2.6332
11	140	146	146	146	146	146	146	144.5	-51.305	8.7829	8.4861	7.9345
12	140	146	146	146	146	146	146	144.5	-40.432	8.2917	8.2535	7.9345
13	140	146	146	146	146	146	146	144.5	-17.334	7.4491	7.5564	7.9345
14	140	146	146	146	146	146	146	144.5	6.935	7.2072	7.3604	7.9345
15	140	146	146	146	146	146	146	144.5	30.992	7.6871	7.9664	7.9345
16	140	146	146	146	146	146	146	144.5	53.6	8.4367	8.5145	7.9345
17	150	146	146	146	146	146	146	147	-58.431	14.029	13.739	13.035
18	150	146	146	146	146	146	146	147	-48.184	13.966	13.611	13.035
19	150	146	146	146	146	146	146	147	-38.449	13.526	13.338	13.035
20	150	146	146	146	146	146	146	147	-27.49	12.984	12.943	13.035
21	150	146	146	146	146	146	146	147	-16.296	12.57	12.571	13.035
22	150	146	146	146	146	146	146	147	-4.938	12.342	12.352	13.035
23	150	146	146	146	146	146	146	147	6.494	12.329	12.369	13.035
24	150	146	146	146	146	146	146	147	17.896	12.527	12.617	13.035
25	150	146	146	146	146	146	146	147	29.171	12.915	13.004	13.035
26	150	146	146	146	146	146	146	147	40.238	13.41	13.396	13.035
27	150	146	146	146	146	146	146	147	51.045	13.836	13.665	13.035
28	160	146	146	146	146	146	146	149.5	-50.489	18.597	18.014	17.329
29	160	146	146	146	146	146	146	149.5	-36.792	18.051	17.6	17.329
30	160	146	146	146	146	146	146	149.5	-15.472	17.092	16.792	17.329
31	160	146	146	146	146	146	146	149.5	6.149	16.879	16.59	17.329
32	160	146	146	146	146	146	146	149.5	27.718	17.534	17.236	17.329
33	160	146	146	146	146	146	146	149.5	48.901	18.467	17.981	17.329
34	170	146	146	146	146	146	146	152	-52.533	21.793	21.099	20.331
35	170	146	146	146	146	146	146	152	-35.426	21.155	20.564	20.331
36	170	146	146	146	146	146	146	152	-14.824	20.27	19.739	20.331
37	170	146	146	146	146	146	146	152	5.882	20.123	19.54	20.331
38	170	146	146	146	146	146	146	152	26.569	20.837	20.183	20.331
39	170	146	146	146	146	146	146	152	47.124	21.707	20.98	20.331
40	180	146	146	146	146	146	146	154.5	-34.332	22.417	21.896	21.703
41	180	146	146	146	146	146	146	154.5	-14.327	21.623	21.076	21.703
42	180	146	146	146	146	146	146	154.5	5.679	21.555	20.883	21.703
43	180	146	146	146	146	146	146	154.5	25.685	22.34	21.511	21.703
44	180	146	146	146	146	146	146	154.5	45.691	23.158	22.331	21.703
45	180	146	146	146	146	146	146	154.5	65.694	23.177	22.522	21.703
46	180	180	180	180	180	180	180	180	15.68	25.269	25.954	26.635
47	180	180	180	180	180	180	180	180	25.68	25.607	26.411	26.635
48	180	180	180	180	180	180	180	180	45.69	26.321	27.366	26.635
49	180	180	180	180	180	180	180	180	65.694	26.604	27.589	26.635
50	180	180	180	180	180	180	180	180	-14.327	25.174	25.904	26.635
51	180	180	180	180	180	180	180	180	-34.332	26.061	26.859	26.635

TABLE S2. *ab-initio* calculated vs $^2J_{\text{Si-O-Si}}$ coupling model. The initial geometry was optimized with RHF/6-311G(d). Individual geometry, after structural constraint on Ω_0, Ω_k and ϕ, was not optimized. All Si-O bond distances were fixed to 1.6 Å and O-Si-O intra-tetrahedral angle set to 109.5°.

Index	$\Omega_0/1^\circ$	$\Omega_k/1^\circ$						$\overline{\langle\Omega\rangle}/1^\circ$	$\phi/1^\circ$	$^2J_{\text{Si-O-Si}}$-coupling /Hz		
		Ω_1	Ω_2	Ω_3	Ω_4	Ω_5	Ω_6			*ab-initio*	$J(\Omega_0, \overline{\langle\Omega\rangle}, \phi)$	$J(\Omega_0, \overline{\langle\Omega\rangle})$
52	120	120	120	120	120	120	120	120	8.237	-2.4502	-3.3223	-3.0199
53	120	130	130	130	130	130	130	127.5	8.237	-2.3752	-3.0189	-2.6976
54	120	140	140	140	140	140	140	135	8.237	-2.1224	-2.7155	-2.3753
55	120	146	146	146	146	146	146	139.5	8.237	-1.9657	-2.5334	-2.1819
56	120	150	150	150	150	150	150	142.5	8.237	-1.8819	-2.412	-2.0529
57	120	160	160	160	160	160	160	150	8.237	-1.6123	-2.1086	-1.7306
58	120	170	170	170	170	170	170	157.5	8.237	-1.2821	-1.8052	-1.4083
59	120	180	180	180	180	180	180	165	8.237	-1.083	-1.5017	-1.0859
60	130	120	120	120	120	120	120	122.5	7.5	1.4423	0.74504	1.1487
61	130	130	130	130	130	130	130	130	7.5	1.6351	1.2913	1.7196
62	130	140	140	140	140	140	140	137.5	7.5	1.9939	1.8376	2.2906
63	130	146	146	146	146	146	146	142	7.5	2.2193	2.1653	2.6332
64	130	150	150	150	150	150	150	145	7.5	2.3653	2.3838	2.8616
65	130	160	160	160	160	160	160	152.5	7.5	2.762	2.9301	3.4326
66	130	170	170	170	170	170	170	160	7.5	3.2326	3.4764	4.0035
67	130	180	180	180	180	180	180	167.5	7.5	3.6555	4.0226	4.5745
68	140	120	120	120	120	120	120	125	6.935	5.8964	5.2636	5.7602
69	140	130	130	130	130	130	130	132.5	6.935	6.2592	6.07	6.5965
70	140	140	140	140	140	140	140	140	6.935	6.8246	6.8765	7.4327
71	140	146	146	146	146	146	146	144.5	6.935	7.2072	7.3604	7.9345
72	140	150	150	150	150	150	150	147.5	6.935	7.4552	7.6829	8.269
73	140	160	160	160	160	160	160	155	6.935	8.0411	8.4894	9.1052
74	140	170	170	170	170	170	170	162.5	6.935	8.722	9.2958	9.9415
75	140	180	180	180	180	180	180	170	6.935	9.3362	10.102	10.778
76	150	120	120	120	120	120	120	127.5	6.494	10.354	9.6437	10.221
77	150	130	130	130	130	130	130	135	6.494	10.962	10.692	11.304
78	150	140	140	140	140	140	140	142.5	6.494	11.771	11.74	12.386
79	150	146	146	146	146	146	146	147	6.494	12.329	12.369	13.035
80	150	150	150	150	150	150	150	150	6.494	12.696	12.789	13.468
81	150	160	160	160	160	160	160	157.5	6.494	13.527	13.837	14.55
82	150	170	170	170	170	170	170	165	6.494	14.448	14.885	15.633
83	150	180	180	180	180	180	180	172.5	6.494	15.182	15.933	16.715
84	160	120	120	120	120	120	120	130	6.149	14.194	13.359	14.002
85	160	130	130	130	130	130	130	137.5	6.149	15.085	14.602	15.282
86	160	140	140	140	140	140	140	145	6.149	16.154	15.844	16.561
87	160	146	146	146	146	146	146	149.5	6.149	16.879	16.59	17.329
88	160	150	150	150	150	150	150	152.5	6.149	17.361	17.087	17.841
89	160	160	160	160	160	160	160	160	6.149	18.462	18.329	19.121
90	160	170	170	170	170	170	170	167.5	6.149	19.567	19.572	20.4
91	160	180	180	180	180	180	180	175	6.149	20.308	20.814	21.68
92	170	120	120	120	120	120	120	132.5	5.882	16.907	15.984	16.674
93	170	130	130	130	130	130	130	140	5.882	18.015	17.352	18.081
94	170	140	140	140	140	140	140	147.5	5.882	19.278	18.719	19.487
95	170	146	146	146	146	146	146	152	5.882	20.123	19.54	20.331
96	170	150	150	150	150	150	150	155	5.882	20.688	20.087	20.894
97	170	160	160	160	160	160	160	162.5	5.882	21.978	21.455	22.301
98	170	170	170	170	170	170	170	170	5.882	23.156	22.822	23.707
99	170	180	180	180	180	180	180	177.5	5.882	23.795	24.19	25.114
100	180	120	120	120	120	120	120	135	5.679	18.298	17.216	17.932
101	180	130	130	130	130	130	130	142.5	5.679	19.451	18.626	19.382
102	180	140	140	140	140	140	140	150	5.679	20.697	20.037	20.833
103	180	146	146	146	146	146	146	154.5	5.679	21.555	20.883	21.703
104	180	150	150	150	150	150	150	157.5	5.679	22.13	21.448	22.283
105	180	160	160	160	160	160	160	165	5.679	23.44	22.858	23.734
106	180	170	170	170	170	170	170	172.5	5.679	24.552	24.269	25.184
107	180	180	180	180	180	180	180	180	5.679	25.017	25.68	26.635

TABLE S3. *ab-initio* calculated vs $^2J_{\text{Si-O-Si}}$ coupling model. Individual geometry, after structural constraint on Ω_0 and Ω_k, was optimized using RHF/6-311G(d). The *ab-initio* J-coupling were then evaluated on the optimized geometry and compare with Eq. (19) of the main document. Excellent agreement in J-coupling model and *ab-initio* result is observed. All Si-O bond distances were fixed to 1.6 Å and O-Si-O intra-tetrahedral angle set to 109.5°.

Index	$\Omega_0/1^\circ$	$\Omega_k/1^\circ$						$\overline{\langle\Omega\rangle}/1^\circ$	$\phi/1^\circ$	$^2J_{\text{Si-O-Si}}$-coupling /Hz		
		Ω_1	Ω_2	Ω_3	Ω_4	Ω_5	Ω_6		optimized	*ab-initio*	$J(\Omega_0, \overline{\langle\Omega\rangle}, \phi)$	$J(\Omega_0, \overline{\langle\Omega\rangle})$
108	130	142	142	142	142	142	142	139	48.553	2.374	2.8141	2.4048
109	140	142	142	142	142	142	142	141.5	-3.63	7.1588	7.0094	7.6
110	150	142	142	142	142	142	142	144	-1.01	12.333	11.911	12.602
111	160	142	142	142	142	142	142	146.5	-48.131	18.823	17.438	16.817
112	170	142	142	142	142	142	142	149	-43.526	21.655	20.298	19.769
113	180	142	142	142	142	142	142	151.5	-163.34	22.695	21.663	21.123
114	130	146	146	146	146	146	146	142	-51.352	2.2449	3.0886	2.6332
115	140	146	146	146	146	146	146	144.5	69.457	8.2131	8.4749	7.9345
116	150	146	146	146	146	146	146	147	6.494	12.329	12.369	13.035
117	160	146	146	146	146	146	146	149.5	-43.389	18.997	17.832	17.329
118	170	146	146	146	146	146	146	152	-44.749	22.294	20.911	20.331
119	180	146	146	146	146	146	146	154.5	-158.46	23.025	22.07	21.703
120	130	149	149	149	149	149	149	144.25	-53.188	2.323	3.2866	2.8045
121	140	149	149	149	149	149	149	146.75	68.928	8.0614	8.7422	8.1853
122	150	149	149	149	149	149	149	149.25	-44.896	14.262	13.864	13.36
123	160	149	149	149	149	149	149	151.75	-40.024	19.09	18.109	17.713
124	170	149	149	149	149	149	149	154.25	-36.953	22.181	21.053	20.753
125	180	149	149	149	149	149	149	156.75	-63.423	24.16	22.994	22.138
126	120	178	178	178	178	178	178	163.5	-73.729	-0.84366	-0.80904	-1.1504
127	130	178	178	178	178	178	178	166	-69.237	4.3472	4.9844	4.4603
128	140	178	178	178	178	178	178	168.5	-69.038	10.709	11.248	10.61
129	150	178	178	178	178	178	178	171	-55.352	16.639	17.296	16.498
130	160	178	178	178	178	178	178	173.5	-40.144	21.178	21.882	21.424
131	170	178	178	178	178	178	178	176	-26.716	24.167	24.668	24.833
132	180	178	178	178	178	178	178	178.5	-142.29	25.249	25.956	26.345

TABLE S4. *ab-initio* calculated vs $^2J_{\text{Si-O-Si}}$ coupling model. The initial geometry was optimized with RHF/6-311G(d). Individual geometry, after structural constraint on Ω_0, Ω_k and ϕ, was not optimized. All Si-O bond distances were fixed to 1.6 Å and O-Si-O intra-tetrahedral angle set to 109.5°.

Index	$\Omega_0/1^\circ$	$\Omega_k/1^\circ$						$\overline{\langle\Omega\rangle}/1^\circ$	$\phi/1^\circ$	$^2J_{\text{Si-O-Si}}$-coupling /Hz		
		Ω_1	Ω_2	Ω_3	Ω_4	Ω_5	Ω_6			*ab-initio*	$J(\Omega_0, \overline{\langle\Omega\rangle}, \phi)$	$J(\Omega_0, \overline{\langle\Omega\rangle})$
133	140	140	140	140	130	130	130	136.25	6.935	6.5463	6.4733	7.0146
134	140	140	140	140	150	150	150	143.75	6.935	7.1414	7.2797	7.8508
135	140	140	140	140	160	160	160	147.5	6.935	7.4539	7.6829	8.269
136	140	140	140	140	170	170	170	151.25	6.935	7.7772	8.0862	8.6871
137	140	150	150	150	130	130	130	140	6.935	6.867	6.8765	7.4327
138	140	150	150	150	140	140	140	143.75	6.935	7.1414	7.2797	7.8508
139	140	150	150	150	160	160	160	151.25	6.935	7.7665	8.0862	8.6871
140	140	150	150	150	170	170	170	155	6.935	8.0846	8.4894	9.1052
141	150	130	146	146	146	146	146	145	6.494	11.882	12.09	12.747
142	150	140	146	146	146	146	146	146.25	6.494	12.129	12.264	12.927
143	150	150	146	146	146	146	146	147.5	6.494	12.47	12.439	13.107
144	150	160	146	146	146	146	146	148.75	6.494	12.848	12.614	13.288
145	150	170	146	146	146	146	146	150	6.494	13.223	12.789	13.468
146	120	154.5	153.24	142.43	158.36	134.56	157.87	142.62	47.643	-2.1903	-1.7321	-2.0478
147	130	157.08	153.88	145.05	160.56	135.83	157.46	146.23	50.461	2.3991	3.4132	2.9554
148	140	160.95	155.8	147.36	161.25	137.16	153.78	149.54	51.534	8.11	9.0703	8.4962
149	150	164.5	159.12	148.42	160.44	138.09	149.49	152.51	52.6	13.882	14.508	13.83
150	160	158.21	163.61	149.71	158.25	139.28	147.48	154.57	55.06	18.593	18.973	18.194
151	170	153.31	166.12	149.46	157.43	140.91	144.64	156.48	56.761	21.393	22.015	21.172
152	125	142	156	160	158	149	161	147	7.845	0.10924	0.060112	0.48901
153	135	142	156	160	158	149	161	149.5	7.2	4.9043	5.3085	5.8538
154	145	142	156	160	158	149	161	152	6.701	10.224	10.705	11.353

TABLE S4. ...continued. *ab-initio* calculated vs $^2J_{\text{Si-O-Si}}$ coupling model, continued. The initial geometry was optimized with RHF/6-311G(d). Individual geometry, after structural constraint on Ω_0, Ω_k and ϕ, was not optimized. All Si-O bond distances were fixed to 1.6 Å and O-Si-O intra-tetrahedral angle set to 109.5°.

Index	$\Omega_0/1^\circ$	$\Omega_k/1^\circ$						$\overline{\langle\Omega\rangle}/1^\circ$	$\phi/1^\circ$	$^2J_{\text{Si-O-Si}}$-coupling /Hz		
		Ω_1	Ω_2	Ω_3	Ω_4	Ω_5	Ω_6			*ab-initio*	$J(\Omega_0, \overline{\langle\Omega\rangle}, \phi)$	$J(\Omega_0, \overline{\langle\Omega\rangle})$
155	155	142	156	160	158	149	161	154.5	6.311	15.398	15.572	16.307
156	165	142	156	160	158	149	161	157	6.007	19.632	19.344	20.144
157	175	142	156	160	158	149	161	159.5	5.772	22.186	21.594	22.436
158	170	145	155	160	167	172	161	162.5	5.882	21.671	21.455	22.301
159	170	137	170	153	150.1	179.9	170	162.5	5.882	20.741	21.455	22.301
160	170	157	166	137	166	173	161	162.5	5.882	21.563	21.455	22.301
161	170	146	164	150	162	168	170	162.5	5.882	21.491	21.455	22.301
162	160	145	155	160	167	172	161	160	6.149	18.143	18.329	19.121
163	160	137	170	153	150.1	179.9	170	160	6.149	17.095	18.329	19.121
164	160	157	166	137	166	173	161	160	6.149	18.127	18.329	19.121
165	160	146	164	150	162	168	170	160	6.149	17.913	18.329	19.121
166	150	145	155	160	167	172	161	157.5	6.494	13.23	13.837	14.55
167	150	137	170	153	150.1	179.9	170	157.5	6.494	12.175	13.837	14.55
168	150	157	166	137	166	173	161	157.5	6.494	13.275	13.837	14.55
169	150	146	164	150	162	168	170	157.5	6.494	12.964	13.837	14.55
170	130	145	155	160	167	172	161	152.5	7.502	2.5666	2.9301	3.4326
171	130	137	170	153	150.1	179.9	170	152.5	7.502	1.8455	2.9301	3.4326
172	130	157	166	137	166	173	161	152.5	7.502	2.6513	2.9301	3.4326
173	130	146	164	150	162	168	170	152.5	7.502	2.3541	2.9301	3.4326
174	180	145	155	160	167	172	161	165	5.679	23.192	22.858	23.734
175	180	137	170	153	150.1	179.9	170	165	5.679	22.472	22.858	23.734
176	180	157	166	137	166	173	161	165	5.679	22.973	22.858	23.734
177	180	146	164	150	162	168	170	165	5.679	23.06	22.858	23.734
178	135	164	155	140	150	166	172	152.12	7.2	5.1271	5.5453	6.1002
179	145	164	155	140	150	166	172	154.62	6.701	10.523	11.031	11.691
180	155	164	155	140	150	166	172	157.12	6.311	15.748	15.976	16.723
181	165	164	155	140	150	166	172	159.62	6.007	19.973	19.804	20.617
182	175	164	155	140	150	166	172	162.12	5.772	22.458	22.084	22.939
183	127.5	135.6	142.8	161.2	155.4	147.3	169.8	145.89	7.668	1.1973	1.2069	1.6604
184	132.5	135.6	142.8	161.2	155.4	147.3	169.8	147.14	7.346	3.5995	3.8128	4.324
185	142.5	135.6	142.8	161.2	155.4	147.3	169.8	149.64	6.814	8.8003	9.1787	9.7959
186	152.5	135.6	142.8	161.2	155.4	147.3	169.8	152.14	6.399	13.998	14.183	14.89
187	162.5	135.6	142.8	161.2	155.4	147.3	169.8	154.64	6.076	18.462	18.233	19.01
188	172.5	135.6	142.8	161.2	155.4	147.3	169.8	157.14	5.825	21.434	20.87	21.695
189	120	168.34	168.34	168.34	169.06	169.06	169.06	156.53	-68.642	-0.50969	-1.0596	-1.4502
190	129.9	168.34	168.34	168.34	169.06	169.06	169.06	159	-63.499	4.9418	4.428	3.8716
191	130	172.78	172.78	172.78	173.11	173.11	173.11	162.21	-63.442	4.7433	4.7408	4.1717
192	140	177.8	177.8	177.8	177.24	177.24	177.24	168.14	-59.26	10.655	11.284	10.57
193	150	175.4	175.4	175.4	178.13	178.13	178.13	170.07	-57	17.058	17.172	16.365
194	160	179.1	179.1	179.1	177.75	177.75	177.75	173.82	-53.18	22.027	22.327	21.478
195	170	179.97	179.97	179.97	179.73	179.73	179.73	177.39	-51.021	25.272	25.957	25.093
196	180	178.58	178.58	178.58	178.68	178.68	178.68	178.97	-49.354	26.525	27.279	26.436
197	140	145	155	160	167	172	161	155	6.935	7.7815	8.4894	9.1052
198	140	137	170	153	150.1	179.9	170	155	6.935	6.8387	8.4894	9.1052
199	140	157	166	137	166	173	161	155	6.935	7.8553	8.4894	9.1052
200	140	146	164	150	162	168	170	155	6.935	7.5261	8.4894	9.1052

TABLE S5. *ab-initio* calculated vs $^2J_{\text{Si-O-Si}}$ coupling model from Sigma-2

Index	$\Omega_0/1^\circ$	$\Omega_k/1^\circ$						$\overline{\langle\Omega\rangle}/1^\circ$	$\phi/1^\circ$	$^2J_{\text{Si-O-Si}}$-coupling /Hz		
		Ω_1	Ω_2	Ω_3	Ω_4	Ω_5	Ω_6			*ab-initio*	$J(\Omega_0, \overline{\langle\Omega\rangle}, \phi)$	$J(\Omega_0, \overline{\langle\Omega\rangle})$
site 2-3	153.45	148.7	153.45	148.7	172.76	153.45	160.8	155.595	0.47	16.0	15.035	15.035
site 1-3	172	137.2	158.21	158.21	160.8	153.45	153.45	158.165	-0.45	22.07	20.958	20.958
site 4-1	137.2	158.21	172.26	158.21	148.78	152.04	148.74	151.575	0.0	6.48	6.552	6.552
site 4-2	148.74	137.2	148.74	152.04	148.74	153.45	153.45	148.8878	27.95	11.09	12.652	11.993